Engineering Structures 319 (2024) 118889

Contents lists available at ScienceDirect

Engineering Structures

journal homepage: www.elsevier.com/locate/engstruct

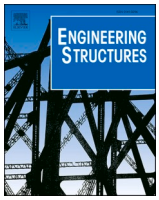

Fire after earthquake assessment of 3D reinforced concrete structures

Ismail Haouach [a], Abdelhak Kada [a], Belkacem Lamri [a], Paulo A.G. Piloto [b,*]

[a] Laboratory Fire Safety Engineering of Constructions and Protection of Their Environment LISICPE, Faculty of Civil Engineering and Architecture, Hassiba Benbouali University of Chlef, Chlef, Algeria
[b] GICoS, Instituto Politécnico de Bragança, Bragança, Portugal

ARTICLE INFO

Keywords:
Fire
Earthquake
Computational Mechanics
Concrete Structures

ABSTRACT

Despite that, an earthquake's occurrence can lead to dramatic effects with significant damage in urban areas, including human and material losses. Fire after an earthquake amplifies the overall impact and becomes a catastrophic event. Most constructions in Algeria are made of reinforced concrete, and current regulations overlook fires after earthquakes. Structural designs are inadequate to handle such events. This study aims to investigate the behaviour of 3D reinforced concrete frames, as part of a residential building, designed according to internal codes, CBA93 and RPA99 v2003. This 3D RC structure is exposed to several load levels of its vertical load bearing capacity. The structural system is assumed to undergo seismic scenarios characterised by various levels of story drift and damage level types. The structure is then exposed to the standard fire ISO834 model. Numerical investigations are carried out for thermo-mechanical analysis using the finite element software ANSYS, taking into account geometric and material non-linearities. Results highlight the significant impact of vertical loads, story drifts, fire scenarios, and structural damage on a building's response to fire following an earthquake. These factors collectively influence the collapse probabilities, underlining the importance of holistic risk assessment in structural design.

1. Introduction

Fires after earthquakes (FAE) have long been recognised as a significant hazard and risk in urban areas. They can cause damage that is worse than the earthquake itself, as they can ignite fires that are difficult to extinguish due to the lack of infrastructure and resources in the aftermath of a disaster [1,2]. Current design codes do not adequately consider the occurrence of FAE, because they are typically based on the assumption that buildings will be able to withstand the earthquake without significant damage. However, even minor earthquake damage can make buildings more vulnerable to fire, disrupting fire suppression systems and creating pathways for fire to spread [3–5]. Hence, a building designed according to current codes is unable to withstand the double action of earthquake and fire, leading to structural damage or even a collapse of the structure.

Researchers have studied the response of reinforced concrete (RC) structures subjected to fire after an earthquake. Mostafaei et al. [6] investigated numerically the FAE performance of an RC six-story building after subjecting it to excitations representing the Kobe Earthquake 1995 records, through a shaking table. They showed that seismic damage to RC elements is an important factor in decreasing the fire resistance time of the building.

Kumar et al. [7] undertook an experimental program involving an RC frame subjected to quasi-static lateral cyclic loading until reaching a pre-defined performance level, followed by a one-hour fire. It was observed that the specimen tested showed considerable resilience, withstanding fire-induced loads without suffering structural collapse. Ab-Kadir et al. [8] conducted a study on an RC frame subjected to FAE witch included both 2D and 3D analyses, revealing considerable differences between the models. Their research highlights the importance of model dimensionality in accurately assessing the structural response of RC frames under combined seismic and fire loading conditions.

Behnam et al. [9] investigated two three-story RC frames, designed according to two seismic performance levels, and exposed to post-seismic fires followed by ISO 834 fire, considering two distinct scenarios. The study examined the combined impact of earthquakes and fires on buildings, revealing the complexity of understanding their simultaneous effects. It presents a methodology to simplify the analysis of this combined effect. The results showed that earthquake-damaged structures exhibited lower fire resistance than their undamaged

* Corresponding author.
E-mail addresses: i.haouach96@univ-chlef.dz (I. Haouach), a.kada@univ-chlef.dz (A. Kada), b.lamri@univ-chlef.dz (B. Lamri), ppiloto@ipb.pt (P.A.G. Piloto).

https://doi.org/10.1016/j.engstruct.2024.118889
Received 7 April 2024; Received in revised form 24 July 2024; Accepted 27 August 2024
Available online 30 August 2024

counterparts. Later, Ni et al. [10] explored the fire resistance of RC structural walls following earthquakes through numerical assessments. They analysed the influence of seismic damage on the fire resistance of these walls. Their findings revealed that, despite a decrease in the load-bearing capacity of earthquake-damaged walls, it remains sufficiently high for most damage types. This suggests that FAE does not pose a significant multi-hazard risk for concrete walls. Vitorino et al. [11] contributed to the understanding of FAE capacity by focusing on the evaluation of RC elements by studying the influence of damage sustained during seismic events and the number of fire frontiers on the temperature of reinforcements. They showed that damage induced by earthquakes and fire fronts significantly affected the fire resistance of RC elements, and its multidimensional nature, highlighting the implications for their structural integrity. Manish et al. [12] analysed a 3D RC frame using ANSYS software, comparing numerical and experimental results, which agreed well. Their study revealed that the frame's vulnerability to fire significantly increases after exposure to earthquake loading, highlighting the importance of assessing FAE impacts on structural integrity. In subsequent research, Vitorino et al. [13] significantly contributed to evaluating the FAE capacity of RC structures. Their investigation specifically addressed the impact of damage location and configuration, as well as the positioning of fire within the structure. The findings indicated that RC frames experiencing damage exhibit reduced fire resistance compared to their undamaged counterparts.

This study investigates the effect of vertical load, story drift, fire scenario, and damage type on the behaviour of three-dimensional 3D RC frames when subjected to FAE. A significant novelty of this research is the consideration of vertical load and story drift as isolated parameters in the context of FAE and the effect of the damage extension, which, to the best of our knowledge, has not been extensively explored in prior studies. Additionally, the analysis of 3D structures provides a more comprehensive understanding of the structural response, moving beyond the traditional two-dimensional 2D assessments. The aim is to develop calibrated models that can accurately predict the structural response of RC frames under these combined effects, contributing valuable insights to the field of the post-earthquake fire of 3D reinforced concrete structures. The analysis is conducted using ISO834 standard fire. Numerical modelling is carried out using ANSYS software, considering GMNIA models (geometrically and materially non-linear imperfection Analysis). The findings offer enhanced insight into the FAE actions and hold significant implications for formulating guidelines aimed at enhancing the safety and performance of RC structures in such circumstances.

2. Methodology

This research will use a performance-based sequential FAE analysis, comprising three main stages. This procedure consists of first applying gravity loads, which remain constant during the analysis. Subsequently, a non-linear seismic analysis is performed. The pushover analysis is used in this study to evaluate the seismic capacity of structures due to its simplicity. Following the pushover analysis of the RC structure, the time step corresponding to each story drift level was identified as the final time step. The data obtained at this stage were used as the initial conditions for the thermo-structural analysis. As per the methodology employed by [2,3,9,11,13], damage resulting from the earthquake was simulated by the assumption that the concrete cover is removed manually in the beams and columns in the beam-column joint region. Two damage types were assumed here, A and B. Damage type A entails the complete removal of the concrete cover over an extension length of 20 cm in both beams and columns. This is based on the calculation of the plastic hinge length as 2/3 h, where h represents the section depth of the member [14]. Given that the damage type is a critical parameter in this study, the length for damage type B was doubled, resulting in a value of 40 cm. Additionally, the scenario of an intact section (undamaged frame) is also considered. The third stage of the analysis involves evaluating the temperature in the concrete and reinforcing steel by applying fire loads under ISO834 fire model [15,16]. At this stage, a transient heat transfer analysis, which is essential for fire safety analysis of reinforced concrete structures, investigates how temperature evolves over time within the structure. The finite element method uses the weighted residual method with the Galerkin approximation to approximate the incremental and iterative solution (nodal temperatures). These nodas temperatures are determined by solving the algebraic system of equations, by iterations. By considering time-varying boundary conditions and temperature dependant thermal properties, such as conductivity, density and specific heat, the analysis predicts temperature field over the structure during a fire event. Following that, a thermo-mechanical analysis is developed, considering the temperature changes from the thermal analysis, as well as the residual stresses and deformations from the seismic analysis, all while keeping the load constant. The slab loads are transferred to the beams, by a distributed load as described in CBA93 [17] and no restraint effect is assumed.

It is important to note that this study does not account for the deformability of the soil. The analysis focuses solely on the effects of FAE on RC structures and hence, the potential impact of soil-structure interaction on the overall behaviour and stability of the structures under such conditions is not considered. Previous research works, such as [18,19], have demonstrated the significant effects of soil-structure interaction. The limitation of the current study should be addressed in a future research.

The structure is considered to have failed when the analysis is unable to converge to a state of equilibrium, using a convergence tolerance based on displacement.

Equilibrium is determined at each time step, involving an iterative process to locate the equilibrium position. The subsequent equilibrium position is influenced by the previous one and the impact of the new incremental thermal load. This procedure runs over time until the structure maintains equilibrium. Verification of the equilibrium position is conducted by assessing the solution's convergence for a tolerance value of 0.001 (m), which is based on the incremental displacement of each node. The non-convergence means that the numerical model is unable to find a stable configuration where the internal stresses balance the applied loads. This model does not consider the soil-structure interaction (influence of soil deformability).

Additionally, the verification of failure involves examining the following conditions, used for elements to assess the ability to support the load during the fire event [20]:

(i) Beam failure to support the load is deemed to have occurred when one of the two criteria has been exceeded. The beam deflection is equal to or greater than 1.5 times the limiting deflection value (D_{lim}), which is given by the Eq. (1)

$$D_{lim} = L^2/400d[mm] \quad (1)$$

- The beam limit values of deflection (D_{lim}) and deflection rate $(dD/dt)_{lim}$ are exceeded, where the deflection rate is determined by Eq. (2):

$$(dD/dt)_{lim} = L^2/9000d[mm/min] \quad (2)$$

Where L is the clear span of the test specimen (in millimetres) and d is the distance between the extreme fibre of the cold design compression zone and that of the cold design tension zone of the structural section (in millimetres).

(i) Column failure to support the load is deemed to have occurred when one of the two criteria has been exceeded:

- The column vertical contraction is equal to or greater than the limiting contraction value (C_{lim}), which is given by the Eq. (3).

$$C_{lim} = h/100[mm] \quad (3)$$

- The column vertical contraction rate $(dC/dt)_{lim}$ is exceeded when reaching the limit defined in Eq. (4).

$$\left(\frac{dC}{dt}\right)_{lim} = 3h/1000[mm/min] \quad (4)$$

The value of h is considered as the initial height (in millimetres).

3. Case study

The case study concerns a structural analysis of a reinforced concrete frame subjected to a standard ISO834 fire after an earthquake action. This frame is taken from a two-story with two equal bays in the horizontal plane, a reinforced concrete residential building designed according to standard regulations [17,21] and built in the town of Chlef, which is classified as a high seismicity zone. The concrete material has a normal strength of 20 MPa and a Poisson's ratio of 0.2, whereas the steel material has a yielding stress of 400 MPa and a Poisson's ratio of 0.3. A concrete cover thickness of 2.5 cm is employed to ensure the preservation of the mechanical properties of the reinforcing steel. Fig. 1 illustrates the geometry and reinforcement cross-sections of the frame.

The structure was subjected to vertical loading under ambient temperature conditions until reaching failure, with the aim of determining its load-bearing capacity.

In the scope of this investigation, four distinct parameters have been considered: vertical loading conditions (load level), story drift, fire scenarios, and the type of concrete damage.

Regarding the vertical loading conditions, the study incorporated seven load levels, ranging from 20 % to 80 % as mentioned in Table 1. Vertical loads were distributed along the beams and applied to the upper nodes of each beam. Four levels of structural story drift were examined: 0 %, 2 %, 3 %, and 4 %, as illustrated in Table 2. During the thermal analysis, the lateral drift data was imported from the model used for the pushover analysis. Concerning the classification of structural damage, two distinct types were investigated: the removal of concrete cover within the nodal region for both beams and columns, with respective extension lengths of 20 cm and 40 cm for damage categories A and B. Notably, the analysis also accounted for the intact section (undamaged structure). Fig. 2 represents the intact and damaged sections of beams and columns. The top concrete cover remained intact in the damaged sections of the beams under the assumption that the earthquake did not affect the integrity of the concrete on the upper surface of the beams, as the slab restrained any potential detachment.

Regarding the fire scenarios, it is assumed that in the first fire scenario (S1), the fire is introduced exclusively at the first level in all compartments, while in the second scenario (S2), the fire is developed at the second level in all compartments. In the third scenario (S3), the fire is fully applied to both levels. The central column is subject to fire from four sides, while the external central columns are exposed to fire from three sides. The corner columns are exposed to fire from two sides. It is worth noting that the central beams are exposed to fire from three sides, while the external beams are exposed from two sides. Fig. 3 and Fig. 4

Table 1
Vertical loads taken into consideration in this study.

Vertical load [%]	Vertical load [kN/m]
20 %	7.2
30 %	10.8
40 %	14.4
50 %	18
60 %	21.6
70 %	25.2
80 %	28.8

Table 2
Values of story drift taken into consideration.

Story drift [%]	1st story drift [mm]	2nd story drift [mm]
0	0	0
2	60	120
3	90	180
4	120	240

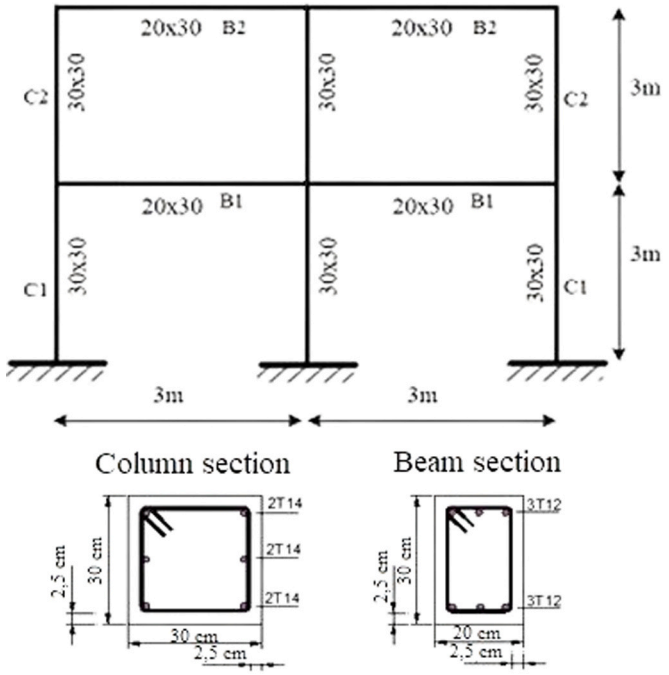

Fig. 1. - Geometry and reinforcement cross-sections of the frame.

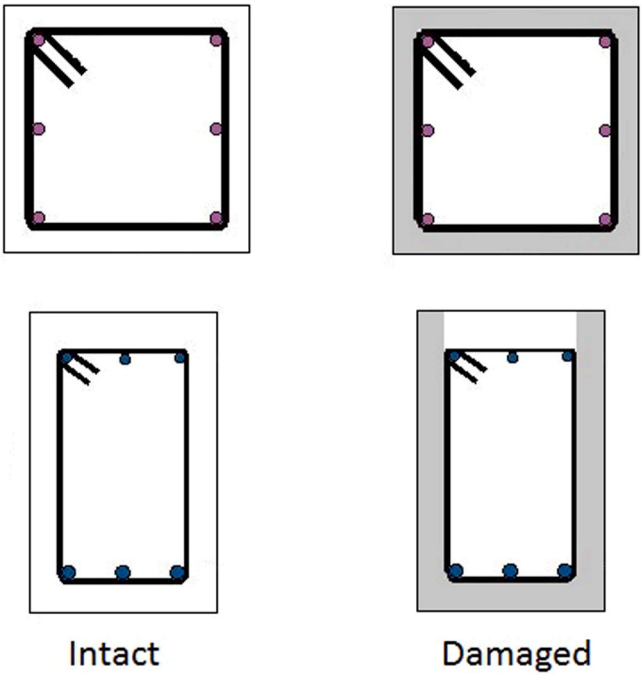

Fig. 2. - Intact and damaged sections of beams and columns.

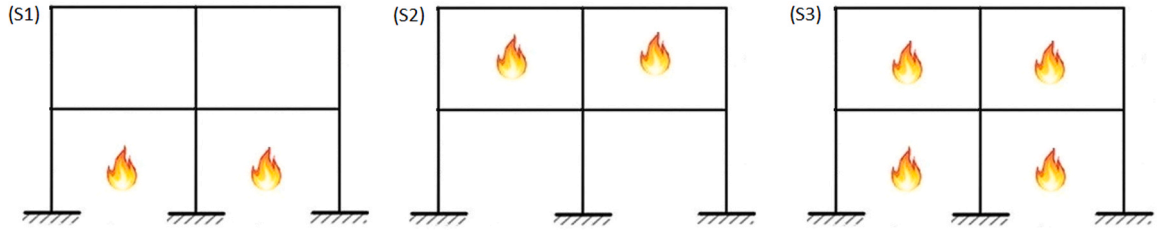

Fig. 3. - Considered fire scenarios: S1 for the first floor, S2 for the second floor, and S3 for both floors.

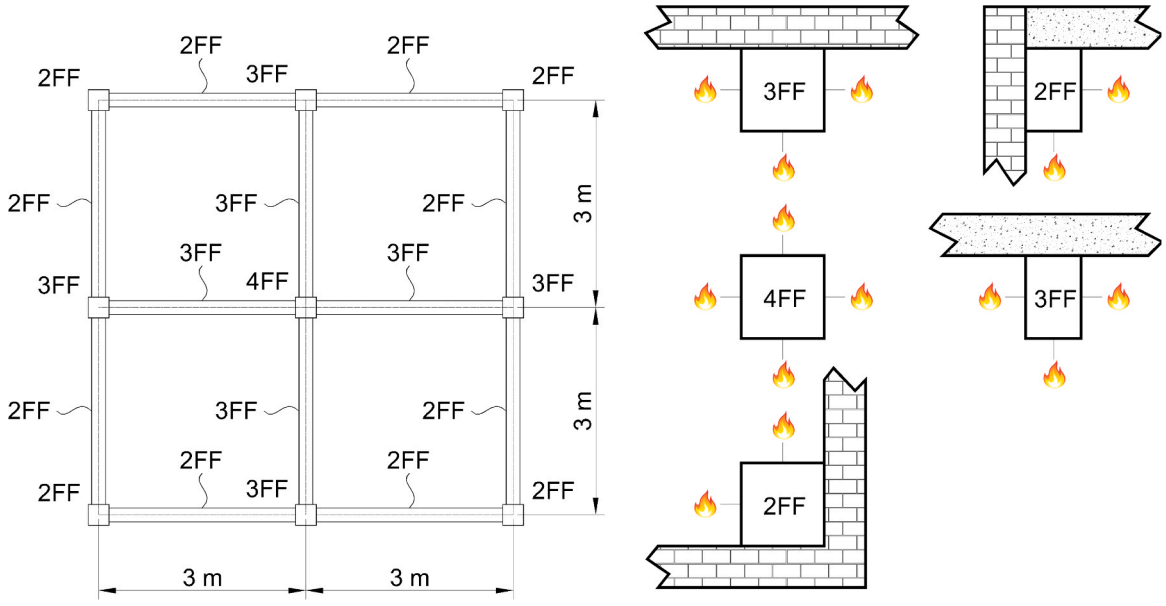

Fig. 4. - Plan view of the 3D structure and the number of fire sides (#FF) of beams and columns.

illustrate the fire scenarios, and the plan view as well as the number of fire frontiers respectively. These thermal boundary conditions, along with the mechanical boundary conditions, may explain the expected deformed mode shapes.

4. Materials properties at elevated temperatures

4.1. *Thermal properties*

Heat transfer in RC elements is highly influenced by the thermal properties of the concrete material which are: density, thermal

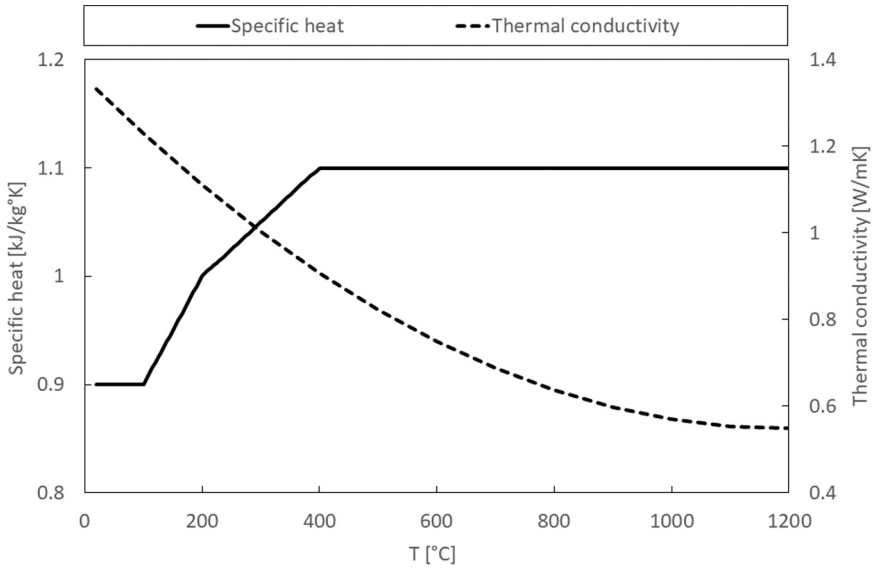

Fig. 5. - Variation of specific heat for a moisture content of 0 % and thermal conductivity of concrete as a function of temperature [24].

conductivity, specific heat and emissivity. The thermal conductivity of concrete depends mainly on the moisture content (here considered as 0 %), the type of aggregates and the percentages of its constitutive materials, while the specific heat of concrete exhibits variability with temperature and moisture content, and the density is slightly affected by temperature which is mainly due to moisture loss during heating [22, 23]. The variation of the specific heat with temperature and the lower limit of thermal conductivity are used in this study. The density of concrete also varies with temperature according to Eurocode 2 part 1–2 [24], as shown in Fig. 5 and Fig. 6.

The specific heat and thermal conductivity depend on temperature as shown in Fig. 7 according to Eurocode 4 part 1–2 [25]. The steel density is assumed to be 7850 [kg/m^3].

4.2. Mechanical properties

High temperatures affect the mechanical properties of concrete [16, 26–28] and steel [29–33]. According to Eurocode 2 [24], the tensile strength of concrete can be neglected. The thermal expansion of concrete depends on the percentage of cement paste, the type of aggregates, as well as the rate of heating and the level of stress [1]. The stress-strain relationships at elevated temperatures are shown in Fig. 10 and Fig. 11 for concrete and steel reinforcement, respectively as per Eurocode 2 part 1–2 [24] utilising Eqs. 5–12. Both materials undergo plasticity, using appropriate yielding criteria.

For the concrete, the stress-strain curve is following the Eq. (5).

$$\text{if}\varepsilon \le \varepsilon_{c1,\theta}\sigma = \frac{3\varepsilon f_{c,\theta}}{\varepsilon_{c1,\theta}\left(2+\left(\frac{\varepsilon}{\varepsilon_{c1,\theta}}\right)^3\right)} \tag{5}$$

When $\varepsilon_{c1,\theta} < \varepsilon \le \varepsilon_{cu1,\theta}$, the perfectly plastic model is assumed. Where σ and ε represent the compressive stress and the strain of the concrete, respectively. The material parameters are presented in Table 3.

For the steel reinforcement, the stress strain curve is following the Eqs. (6–8).

$$\text{if}\varepsilon < \varepsilon_{sp,\theta}\sigma = \varepsilon E_{s,\theta} \tag{6}$$

$$\text{if}\varepsilon_{sp,\theta} \le \varepsilon \le \varepsilon_{sy,\theta}\sigma = f_{sp,\theta} - c + \left(\frac{b}{a}\right)\left[a^2 - \left(\varepsilon_{sy,\theta} - \varepsilon\right)^2\right]^{0.5} \tag{7}$$

$$\text{if}\varepsilon \ge \varepsilon_{sy,\theta}\sigma = f_{sy,\theta} \tag{8}$$

Where σ and ε represent the stress and the strain of the steel reinforcement, respectively. The strain corresponding to the proportional limiting stress is given by Eq. (9), and the strain corresponding to the yield stress is assumed to be $\varepsilon_{sy,\theta} = 0.02$.

$$\varepsilon_{sp,\theta} = f_{sp,\theta} \Big/ E_{s,\theta} \tag{9}$$

The other constitutive parameters are defined according to Eqs. (10–12).

$$a^2 = \left(\varepsilon_{sy,\theta} - \varepsilon_{sp,\theta}\right)\left(\varepsilon_{sy,\theta} - \varepsilon_{sp,\theta} + c/E_{s,\theta}\right) \tag{10}$$

$$b^2 = c\left(\varepsilon_{sy,\theta} - \varepsilon_{sp,\theta}\right)E_{s,\theta} + c^2 \tag{11}$$

$$c = \frac{\left(f_{sy,\theta} - f_{sp,\theta}\right)^2}{\left(\varepsilon_{sy,\theta} - \varepsilon_{sp,\theta}\right)E_{s,\theta} - 2\left(f_{sy,\theta} - f_{sp,\theta}\right)} \tag{12}$$

The constant parameters used for the stress-strain curves are presented in Table 4. Fig. 8 and Fig. 9 illustrate the typical stress-strain curve at elevated temperatures as a result of using Eqs. 5–12 for concrete and steel reinforcement, respectively.

5. Numerical model and validation

The simulation is carried out sequentially, using ANSYS APDL software, with the thermal model for the transient analysis and the mechanical model for the seismic and structural analyses, including material and geometric nonlinearities (GMNIA).

5.1. Finite element model

The thermal analysis is performed using the 8-node SOLID70 finite element for modelling concrete, using linear interpolating functions in space and the full Gauss integration method (2×2x2). The 2-node LINK33 finite element is used to model reinforcing steel, considering linear interpolating functions in the axial direction to conduct heat flow and exact integration. Each node in these elements is assigned with a single degree of freedom (temperature). The convective heat transfer coefficient, α_c, is taken to be equal to 25 [W/m^{2}K] for fire-exposed surfaces and 4 [W/m^{2}K] for unexposed surfaces according to Eurocode 1 part 1–2 [34]. Radiation is also included using the emissivity of the fire equal to $\varepsilon_f = 1$ and considering the emissivity of the exposed material equal to $\varepsilon_m = 0.7$.

The mechanical analysis uses SOLID65 element with 8 nodes and

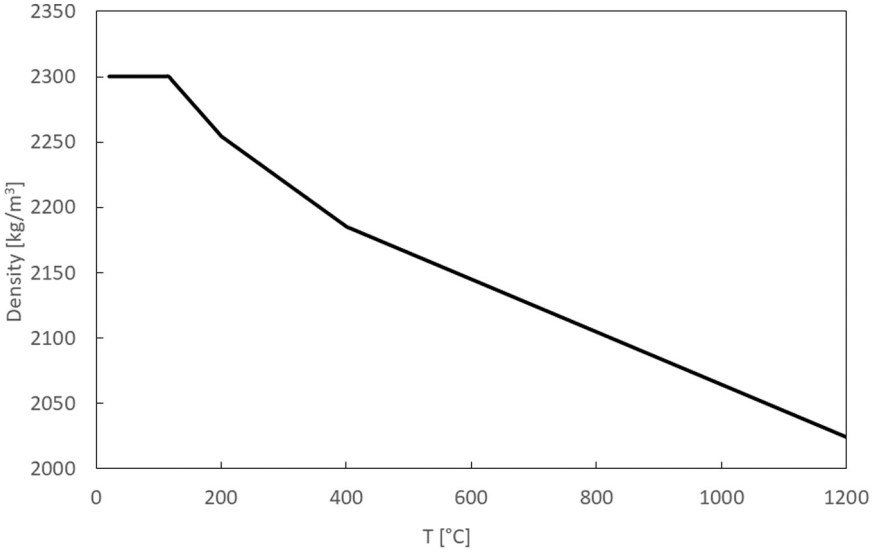

Fig. 6. - Variation of the density of concrete as a function of temperature [24].

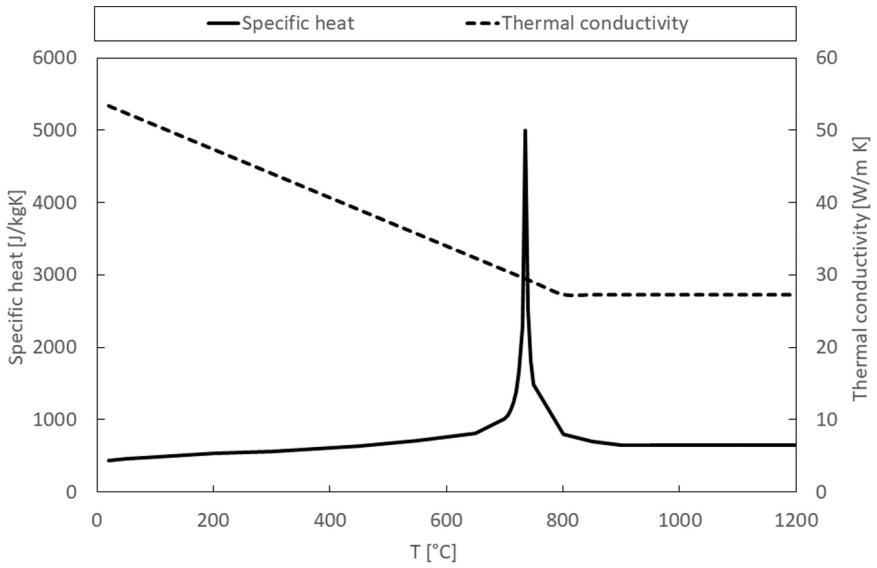

Fig. 7. - Variation of specific heat and thermal conductivity of reinforcement as a function of temperature [25].

Table 3
Values for the main parameters of the stress-strain relationship of the concrete at elevated temperatures (Siliceous aggregates).

Temperature [°C]	$f_{c,\theta}/f_{ck}$ [-]	$\varepsilon_{c1,\theta}$ [-]	$\varepsilon_{cu1,\theta}$ [-]
20	1.00	0.0025	0.0200
100	1.00	0.0040	0.0225
200	0.95	0.0055	0.0250
300	0.85	0.0070	0.0275
400	0.75	0.0100	0.0300
500	0.60	0.0150	0.0325
600	0.45	0.0250	0.0350
700	0.30	0.0250	0.0375
800	0.15	0.0250	0.0400
900	0.08	0.0250	0.0425
1000	0.04	0.0250	0.0450
1100	0.01	0.0250	0.0475
1200	0	-	-

Table 4
Values for the main parameters of the stress-strain relationship of the steel reinforcement at elevated temperatures.

Temperature [°C]	fsy,θ/fyk [-]	fsp,θ/fyk [-]	Es,θ/Es [-]
20	1.00	1.00	1.00
100	1.00	1.00	1.00
200	1.00	0.81	0.90
300	1.00	0.61	0.80
400	1.00	0.42	0.70
500	0.78	0.36	0.60
600	0.47	0.18	0.31
700	0.23	0.07	0.13
800	0.11	0.05	0.09
900	0.06	0.04	0.07
1000	0.04	0.02	0.04
1100	0.02	0.01	0.02
1200	0	0	0

LINK180 element with 2 nodes, both with 3 degrees of freedom for each node. Both finite elements use linear interpolating functions and the full Gauss integration method. The first element is used to model the concrete for its capability of plastic deformation, cracking and crushing [35] and the second for the reinforcement bars considering the translations in the three orthogonal directions, sharing the same nodes from SOLID65.

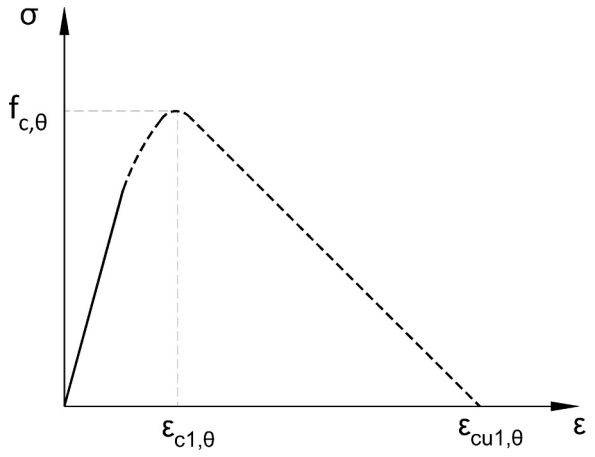

Fig. 8. - Stress-strain relationship model for concrete under compressive loads at elevated temperatures [24].

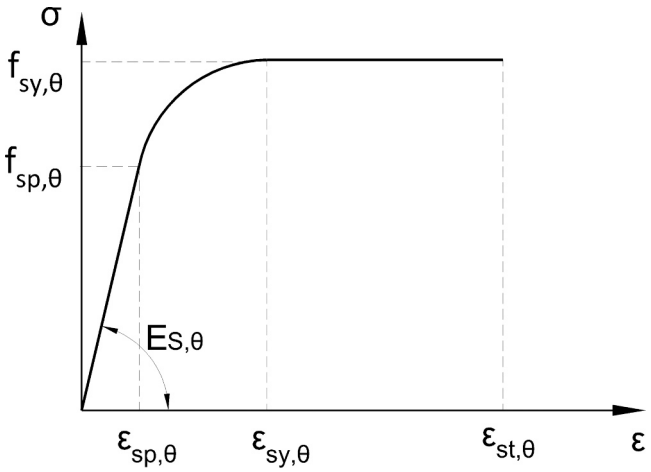

Fig. 9. - Stress-strain relationship model for steel reinforcement at elevated temperatures [24].

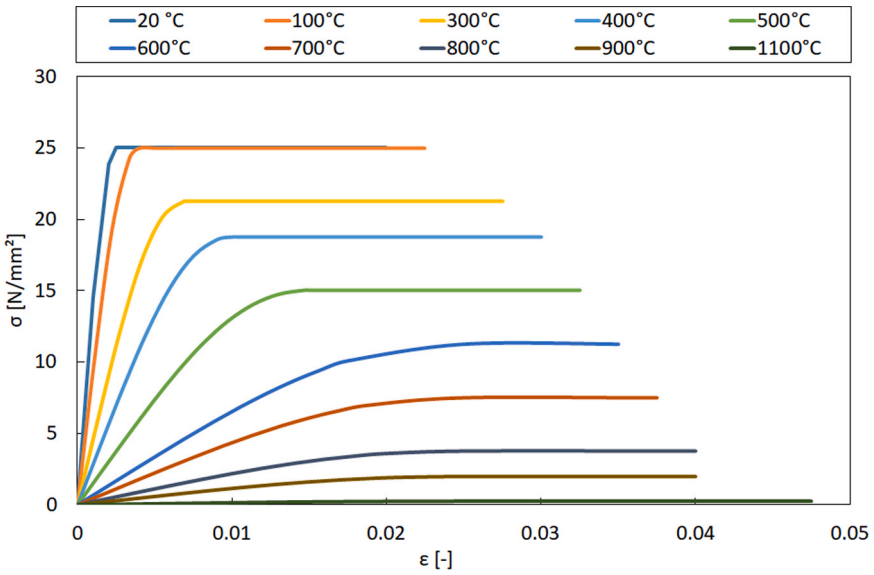

Fig. 10. - Stress-strain curves of siliceous aggregate concrete at elevated temperatures [24].

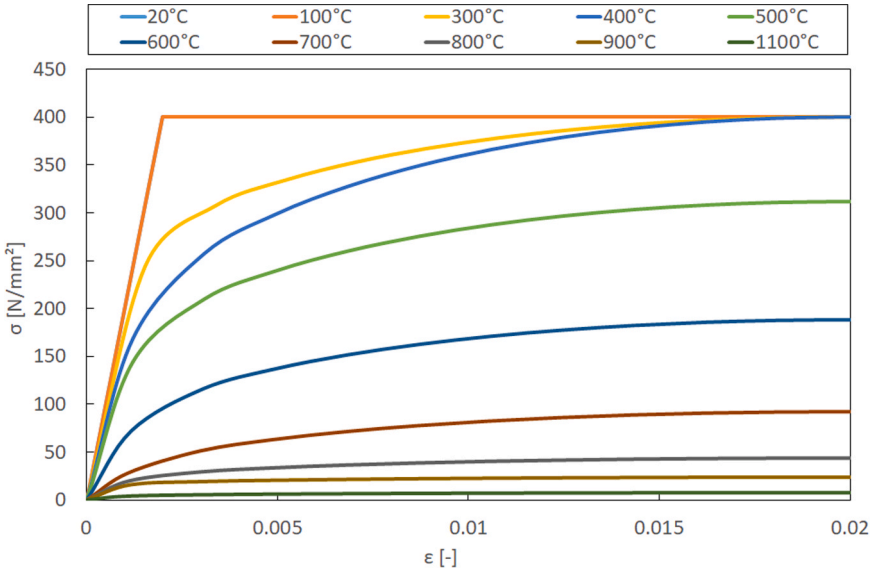

Fig. 11. - Stress-strain curves of S400 steel reinforcement at elevated temperatures [24].

In order to obtain the global response of the structural elements, a perfect contact is assumed between the concrete and the reinforcing steel, neglecting bond slip [36]. Therefore, no specific contact element is assigned. Fig. 12 illustrates the mesh used in the present investigation.

The solution methodology is incremental and iterative, using the Newton–Raphson method, considering a convergence criterion defined by a tolerance limit of 0.001 on the displacement norm, with a reference value of 1 [m].

5.2. Seismic model validation

A single-story reinforced concrete frame, tested experimentally under cyclic loading by Pires [37], is selected to validate the model in seismic analysis. This frame, made of class C20/25 concrete, has a height of 1.625 m and a span of 2.1 m, with cross sections of 15 cm × 20 cm and 15 cm × 15 cm, for the beam and columns, respectively, as shown in Fig. 13. The original study provides information on the use of steel grade S400, while a subsequent conference paper references two distinct steel grades S400 and S500 [38]. Therefore, in this study, two different steel grades S400 and S500 are used for the longitudinal reinforcement and stirrups respectively. Fig. 14 shows the evolution of the lateral force as a function of displacement obtained from the numerical model as well as the experimental test. The accuracy of the numerical was evaluated through the calculation of the relative root-mean-square error (RMSE). In this validation, the RMSE yielded a modest value of 4.23 % during the simulation, emphasising a notable concordance between the numerical predictions and experimental observations. This finding suggests a substantial level of accuracy in the alignment of the two sets of results.

5.3. Thermal model validation

A reinforced concrete beam is taken from the experimental study done by Dwaikat et al. [40] to validate the thermal model by exposing the beam to a standard fire ASTM E119 for 3 h. The dimensions of the beam are 3962 mm, 254 mm and 406 mm in length, width and depth respectively. The beam was monitored by 20 thermocouples type K. The

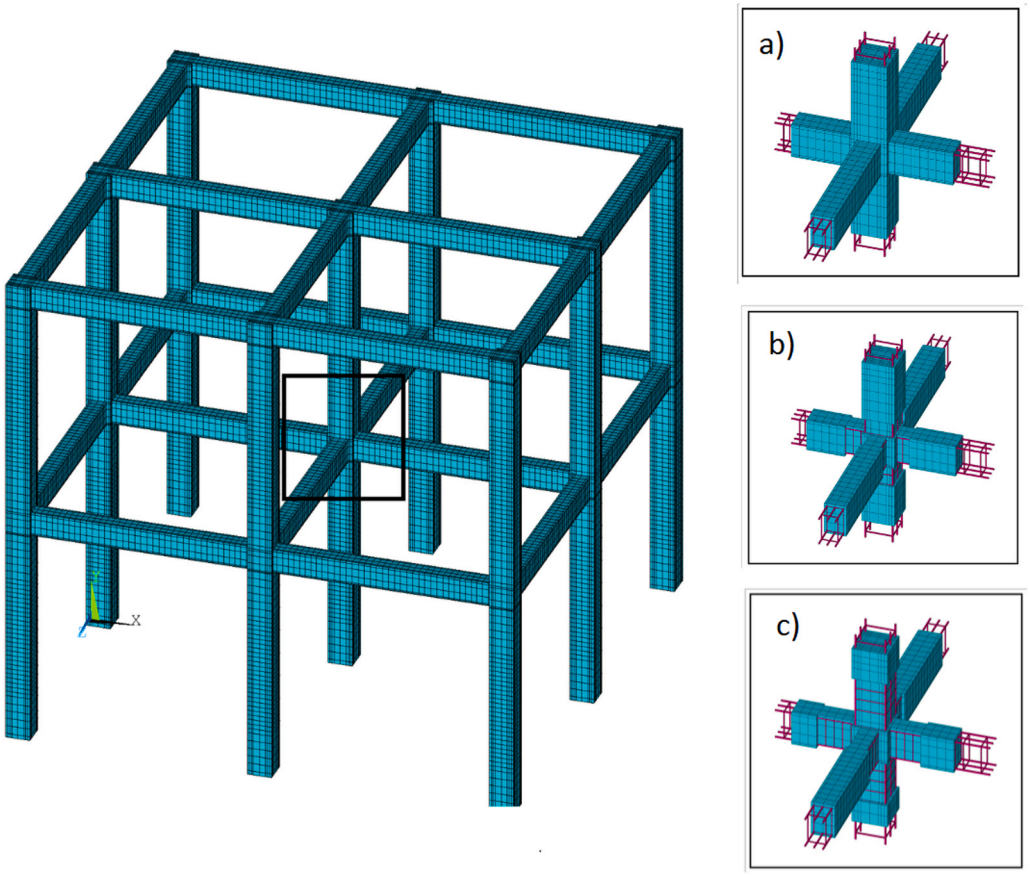

Fig. 12. - Mesh for concrete and reinforcement elements in the developed finite element model; a) Intact section without damage, b) Damage type A, c) Damage type B.

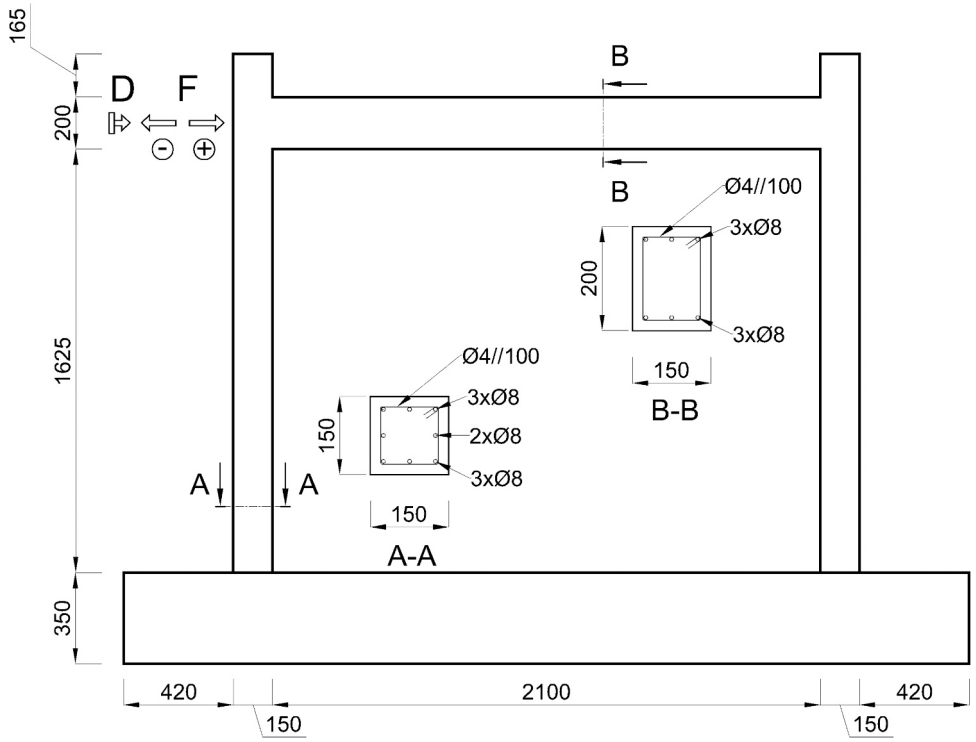

Fig. 13. - Dimensions of the frame employed in the experimental test [39].

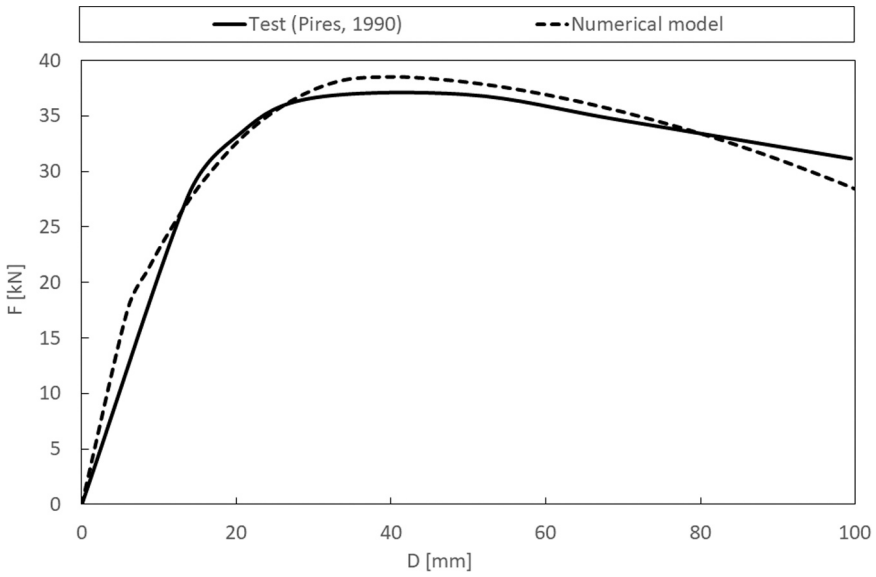

Fig. 14. - Lateral force as a function of displacement - Numerical model and experimental test [39].

Michigan State University furnace was designed to test different conditions regarding temperature and load, see Fig. 15.

Fig. 16 presents the evolution of the temperature as a function of time obtained from the experimental results and from the numerical model at the mid-depth of the cross-section (TC10) and at the level of the longitudinal reinforcement (TC7).

The position of the thermocouples is identified in Fig. 17, using the appropriate nodal location to compare the results. The beam is submitted to fire from three sides, but only the central part is fire exposed (length of 244 cm) as presented in Fig. 18.

A slight discrepancy is observed between the experimental and numerical results. The RMSE values for the rebar (TC7) and the mid-depth of the cross-section (TC10) of the beam were 16.6 °C and 82.7 °C, respectively. Both values are smaller than the threshold of 100 °C, which indicates that the numerical results are in good agreement with the experimental results as referred to in EN 1363–1 [20].

5.4. *Thermo-structural model validation*

The aforementioned reinforced concrete beam which is subjected, at the same time, to thermal loads according to the standard fire ASTM E119 [41] and to two-point mechanical static loads, is used for the thermo-structural validation. Fig. 19 presents a comparison of the deflection at mid-span as a function of time between the test and the numerical model. The relative RMSE was ascertained at 2.86 %, a value suggestive of a marginal discrepancy. This outcome substantiates a good agreement between the numerical simulations and the corresponding experimental results.

Once the numerical models were validated against the experimental test results, they were subsequently applied to the structural analysis. This assures that the models accurately follow the experimental behaviour, providing a reliable basis for further investigation and application in the structural assessment. By utilising these validated numerical models, it was possible to confidently simulate various conditions and predict the performance of the structure under different scenarios, thereby enhancing the robustness and credibility of the study.

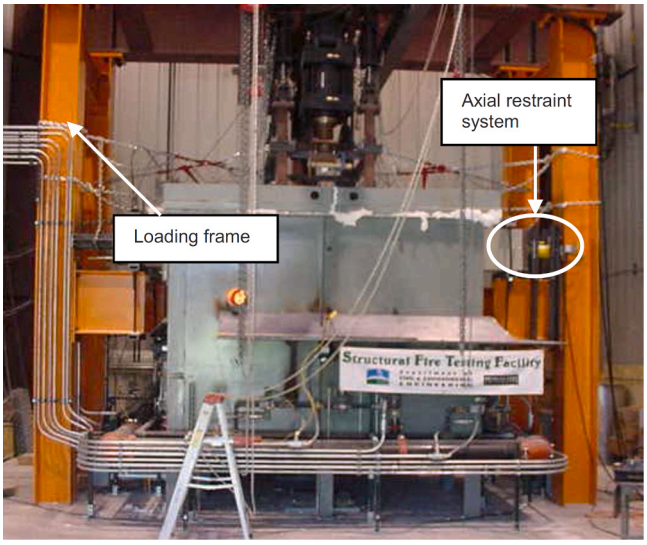

Fig. 15. - Structural fire test furnace at MSU Laboratory [40].

6. Results and discussion

In this section, the findings from the thermal and thermo-structural analyses of RC structures subjected to FAE conditions are presented. A comprehensive examination of the thermal behaviour and structural performance under these combined effects is provided, highlighting key observations and implications for structural safety. The specific results obtained from the analyses are presented, offering insights into the response of the structures under these extreme conditions.

The pushover analysis of the RC structure reveals crucial insights into its seismic performance, demonstrating a balance of strength and ductility. As shown in Fig. 20, the pushover curve, plotting base shear against roof displacement, experiences an upward trend in the elastic phase, reaching a maximum base shear of 491 kN at a roof displacement of 125 mm. Beyond this point, in the plastic phase, the curve exhibits a downward trend, with the base shear decreasing to 386 kN at a roof displacement of 300 mm, indicating significant damage. Despite this reduction in load-bearing capacity, the structure retains some residual strength, ensuring a margin of safety.

Lateral loads were applied at the centre of the structure, specifically at the centre of mass of each floor level. In Fig. 20, the node located at the centre of mass of the top floor was used to measure the roof displacement. The base shear was determined by summing the lateral reactions of all nodes situated at the base of the structure.

Fig. 21 illustrates the temperature profiles of both intact and

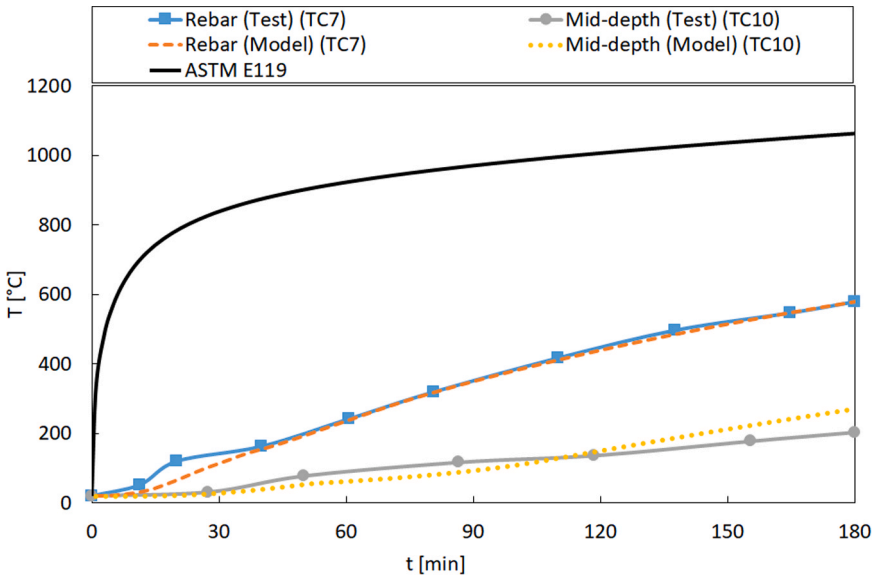

Fig. 16. - Comparison of predicted and measured temperature as a function of time.

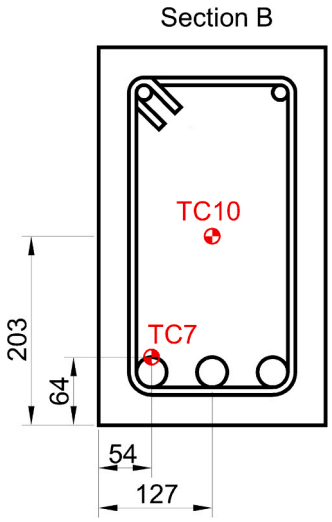

Fig. 17. - Thermocouple location for the mid span of the beam (section B) (Dim. in mm) [40].

damaged beam cross-sections at 60, 120, 180, 240, and 300 min. For the intact beam, the temperature increases rapidly near the exposed surfaces at 60 min, with the core remaining cooler. By 120 min, the heat penetrates further into the core, but a significant temperature gradient persists. At 180 min, while temperatures rise overall, the gradient remains evident. At 240 and 300 min, temperature differences across the cross-section continue, highlighting ongoing thermal gradients and an expected reducing bearing capacity.

In the damaged beam, the temperature profiles indicate faster and more extensive heat penetration due to the absence of the concrete cover. At 60 min, the temperatures are higher due to the sink effect of the rebars, and the gradients are less pronounced when compared to the undamaged beam. By 120 and 180 min, the damaged beam shows higher overall temperatures with persistent gradients. At 240 and 300 min, temperature difference still exists, indicating continued thermal gradients.

Fig. 22 shows the temperature profiles for both intact and damaged column cross-sections over the same time intervals. The undamaged column exhibits a similar pattern to the undamaged beam, with slower heat penetration and persistent temperature gradients. Conversely, the damaged column, similar to the damaged beam, reaches higher temperatures more quickly and displays less pronounced but still evident gradients in temperature. This comparison emphasises the protective role of the concrete cover in both beams and columns, moderating temperature rise under fire conditions.

Fig. 23 illustrates the temperature evolution within the rebar elements across both the damaged and intact cross sections. Within the undamaged section, rebar elements 2, 3, 5, and 6 exhibited temperatures

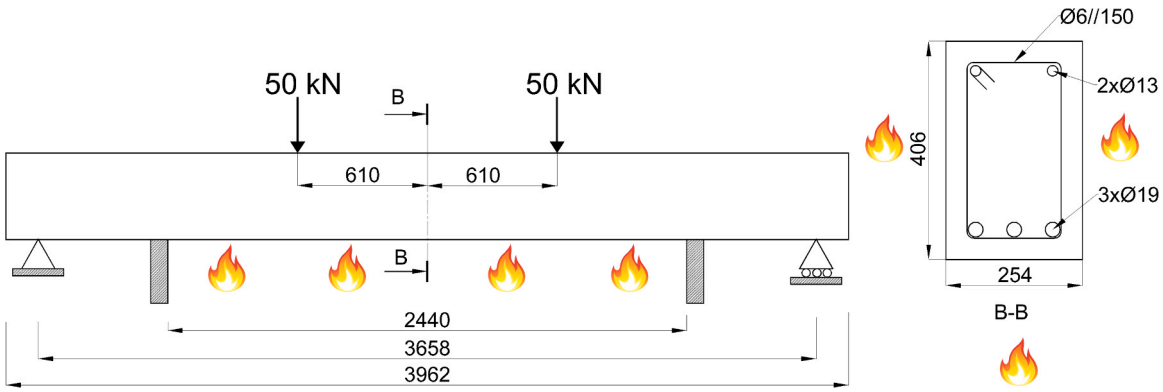

Fig. 18. - Fire exposure details of the beam used for the validation (Dim. in mm).

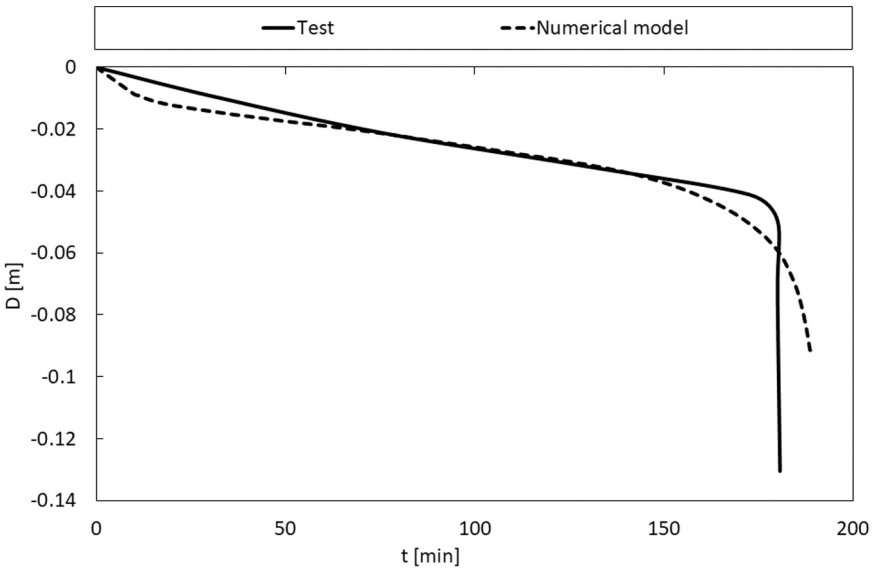

Fig. 19. - Comparison between the measured and predicted mid-span deflection of the beam as a function of time.

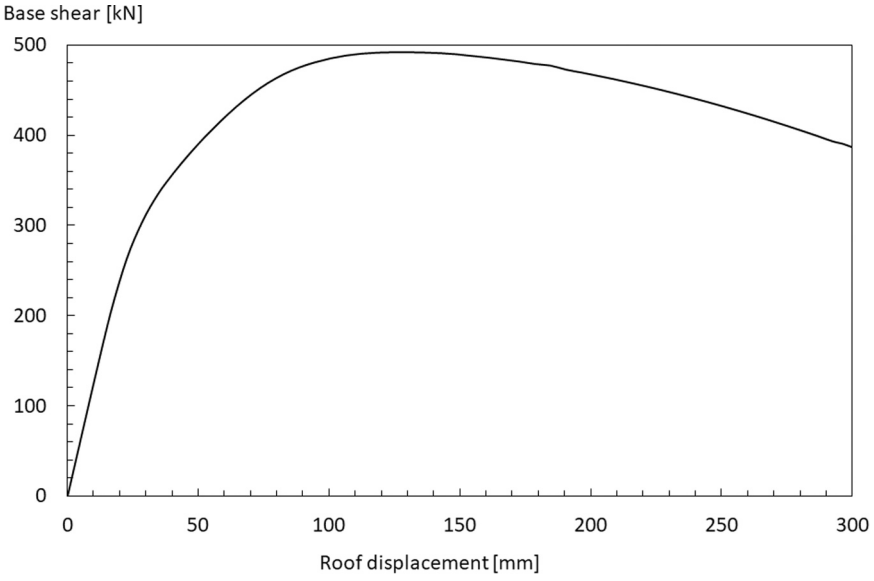

Fig. 20. - Pushover curve of the studied structure (Lateral loads applied at the centre of the structure).

of 408 °C, 553 °C, 105 °C, and 324 °C respectively following a one-hour exposure to fire, while in the damaged section, rebar elements 2, 3, 5, and 6 predicted temperatures of 912 °C, 918 °C, 250 °C, and 854 °C respectively. It should be noted that in both cases, rebar elements 1 and 3 follow similar patterns of evolution, as do rebar elements 4 and 6. This difference highlights the substantial impact that structural damage can have on the thermal response of rebar elements during a fire. The increasing temperatures in the damaged section suggest a decreased capacity for heat dissipation, likely due to compromised material integrity.

It should be noted that in both, the damaged and undamaged sections, rebar elements 1 and 3 follow similar temperature evolution patterns, as do rebar elements 4 and 6. This indicates a consistent behaviour in temperature distribution relative to their positions within the cross-section, regardless of the presence of damage. Such patterns suggest a symmetrical thermal behaviour in rebar elements located symmetrically within the cross-section, which is crucial for understanding the overall structural integrity during fire exposure. These findings emphasise the importance of considering both intact and damaged states in assessing the fire resistance and safety of RC structures.

Fig. 24 depicts the temperature and displacement fields corresponding to the last incremental time step for which equilibrium has been achieved. These results relate to the fire scenario (S1) with a load level of 20 %. This figure provides a comprehensive view of elements, illustrating the temperature and displacement fields throughout the structure. Notably, it can be observed that in the undamaged structure, the displacement is lower than that of the damaged structure with damage type A, and in the latter, the displacement is lower than that of damage type B. This comparison sheds light on the varying degrees of structural response to the imposed conditions.

Figs. 25–27 illustrate the time until collapse as a function of the load level concerning the type of damage and the story drift, for all three fire scenarios S1, S2 and S3 respectively. The fire resistance decreases with the load level as expected for all the cases. For the fire scenario S1, the effect of the story drift shows a big influence on the fire resistance, for

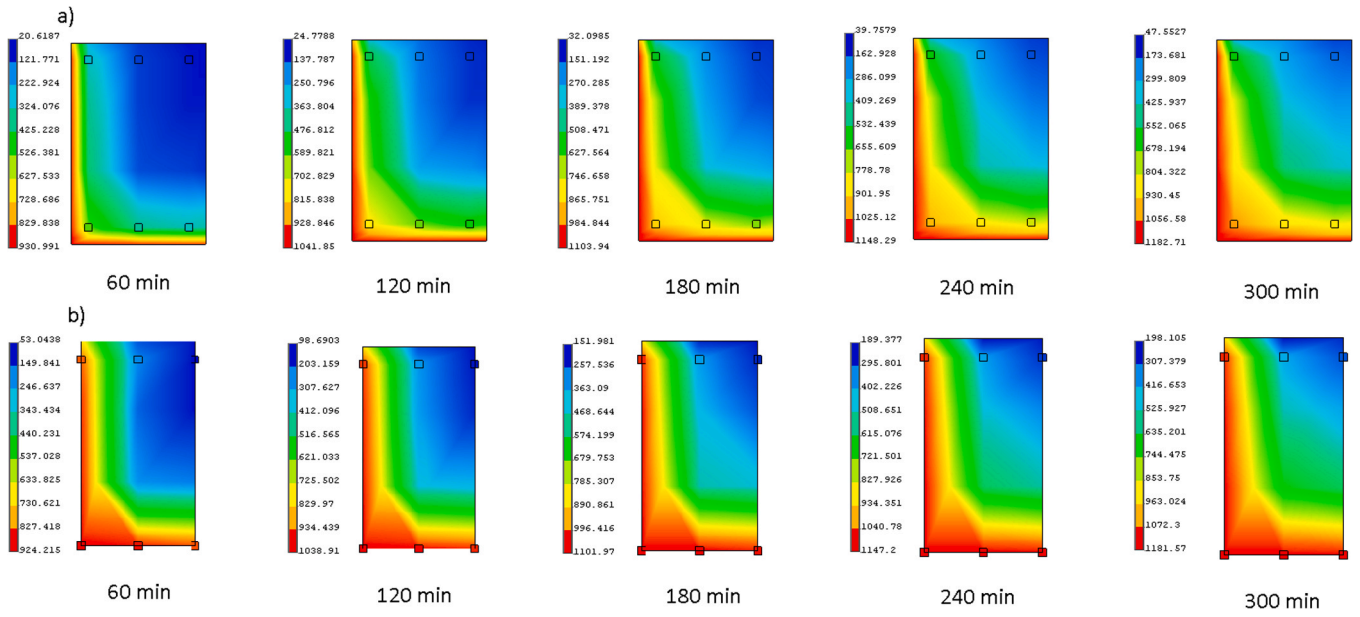

Fig. 21. - Temperature profiles of 2FF beams; a) intact sections, b) damaged sections.

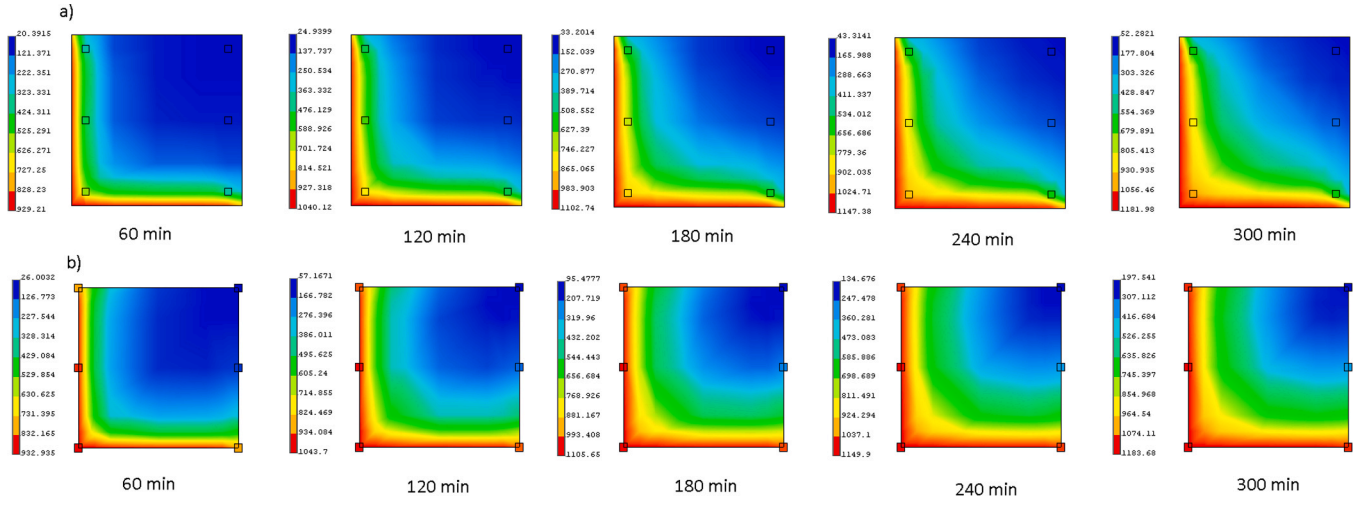

Fig. 22. - Temperature profiles of 2FF columns; a) intact sections, b) damaged sections.

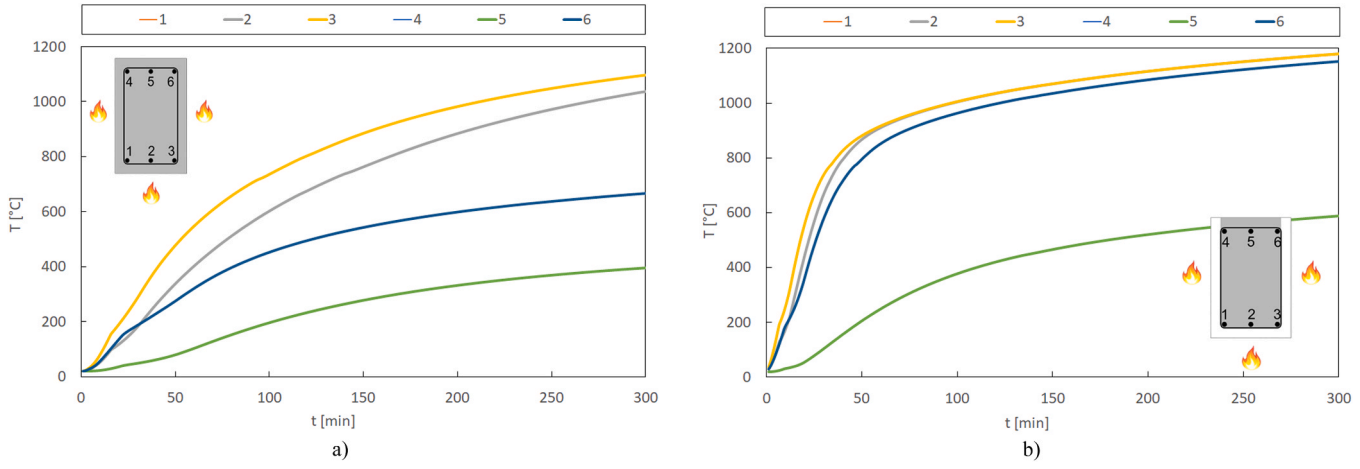

Fig. 23. - Temperature variation of the steel reinforcement of the beams as a function of time: a) intact section, b) damaged section.

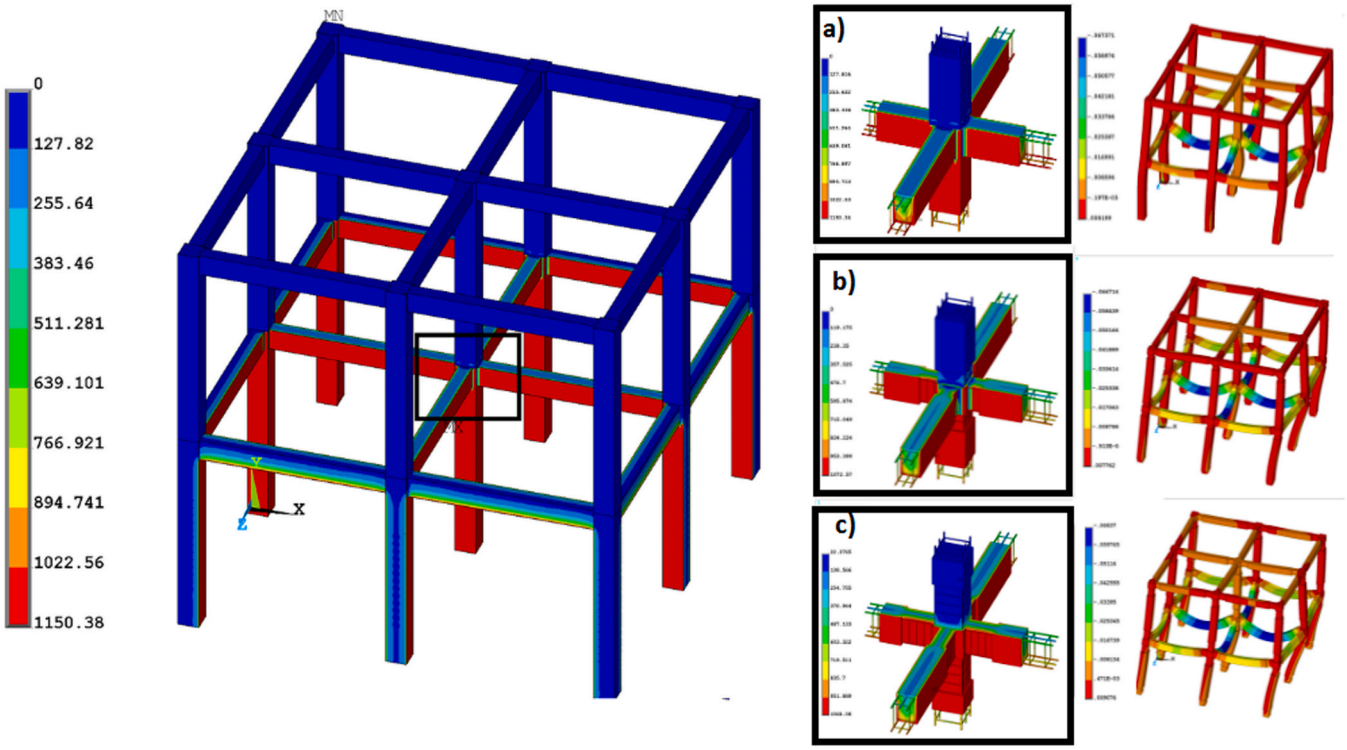

Fig. 24. - Temperature and displacement fields for the ultimate limit state, corresponding fire scenario (S1) for the time reaching the criteria of collapsing member; a) Undamaged structure, b) Structure with damage A, c) Structure with damage B.

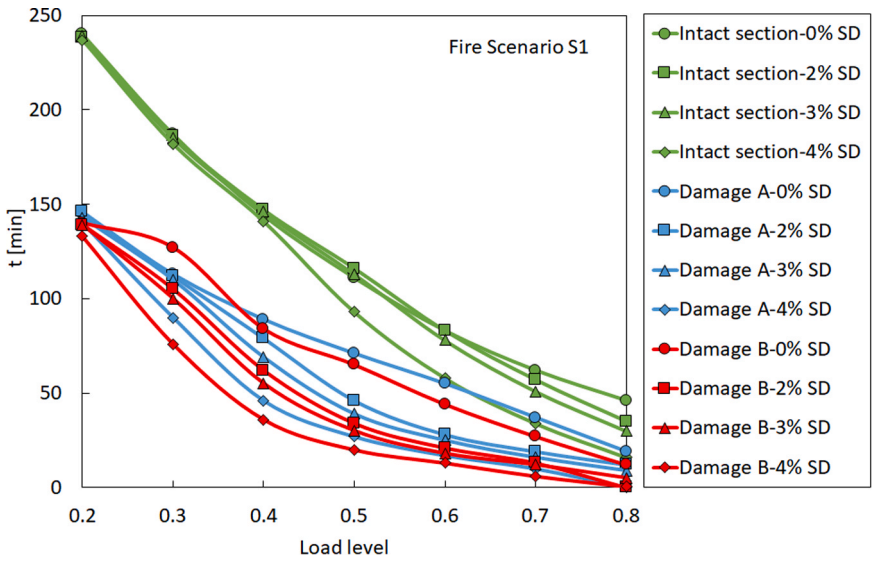

Fig. 25. - Time until collapse as a function of the load level for the fire scenario S1.

the RC structure affected by the damage types A and B. This story drift effect becomes important in the case of undamaged structures when the load level is over 40 %.

As shown in Fig. 26, for the fire scenario S2, the effect of the story drift does not significantly influence the fire resistance, for the RC structure affected by the damage types A and B. There is a big difference in fire resistance (approximately by 100 min), when comparing the undamaged model with both damaged models, type A and type B, for every load level.

The results for the fire scenario S3, highlight again the influence of the fire on the bottom compartments (first level). Almost similar conclusion can be drawn from the effect of fire scenario S1, but with smaller fire resistance for the RC structure for all the load levels and damage types. The effect of the story drifts has a big influence on the fire resistance when considering different types of damage levels that occur in the joints of the structure. The overall ductility of the structure, which is already impacted by seismic displacement and damage, influences the structural stability when exposed to fire following an earthquake. This observation corroborates the findings of the study conducted by Vitorino et al. [42]. According to Dahal et al. [43], the force versus story drift gives an estimate of the overall global stiffness of the system. The decrease in stiffness is one of the most important damages in any extreme event such as a fire. This effect is also noticed in the case of undamaged models, when the load level is higher than 40 %.

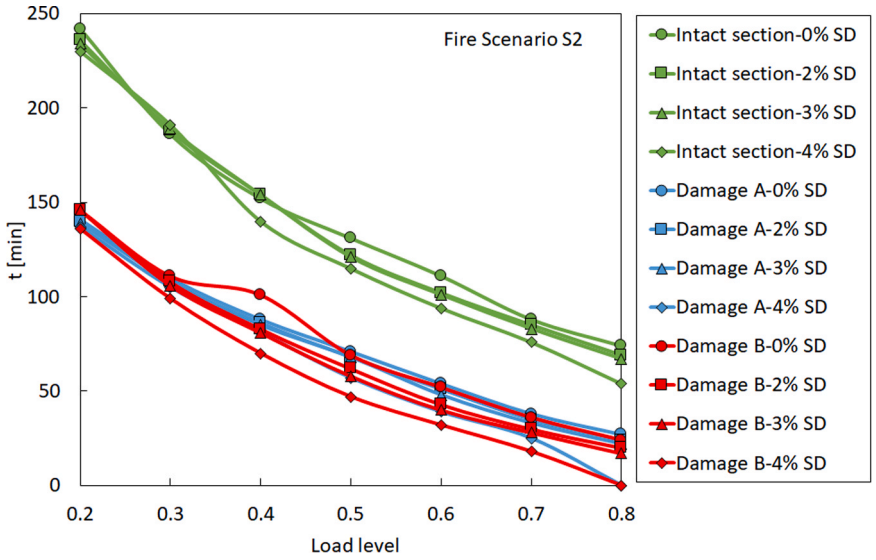

Fig. 26. - Time until collapse as a function of the load level for the fire scenario S2.

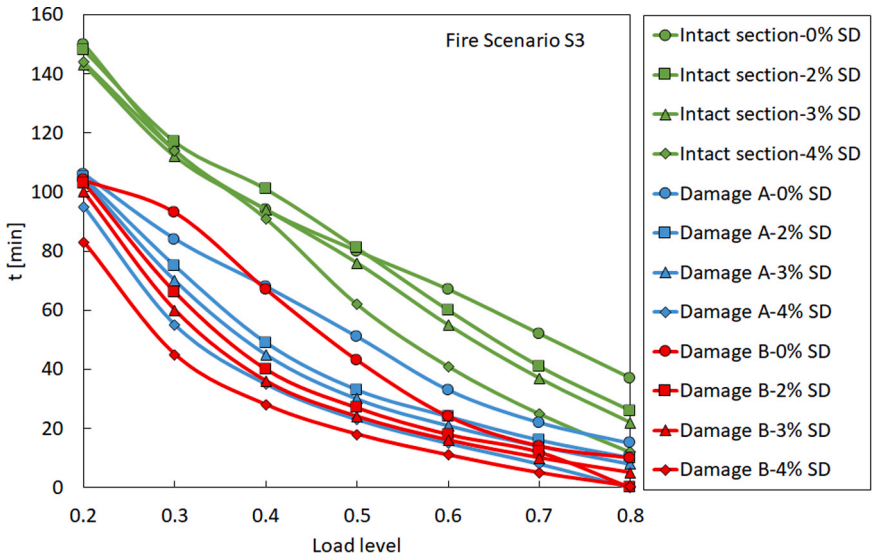

Fig. 27. - Time until collapse as a function of the load level for the fire scenario S3.

The results are also presented as the probability of collapse over time for the various parameters examined in this study. These probabilities are depicted using the Cumulative Distribution Function (CDF), calculated with the following Eqs. (13–15), based on the results presented in Table (appendix).

$$F_X(x_i) = \frac{\text{rank of} x_i}{n} \tag{13}$$

Where $F_X(x_i)$ represents the value of the CDF at the point x_i, x_i denotes the time to collapse for each analysis, and n is the total number of analyses conducted for each parameter.

To adjust the values, the CDF is defined by the integral:

$$F_X(x) = \int_{-\infty}^{x} f_X(x)dx \tag{14}$$

where the probability density function (PDF) $f_X(x)$ is given by Eq. (15).

$$f_X(x) = \frac{1}{\sqrt{2\pi\sigma^2}} \exp\left(-\frac{(x-\mu)^2}{2\sigma^2}\right) \tag{15}$$

In this context, $f_X(x)$ is the probability density function (PDF), μ is the mean value, and σ is the standard deviation.

Fig. 28 illustrates the probability of collapse as a function of time for the different load levels. The graph provides insights into how the probability of collapse evolves over time following a fire after an earthquake. Each curve on the graph represents a different scenario based on the vertical load-bearing capacity of buildings from 20 to 80 %. These curves allow us to compare how buildings with varying capacities respond to the combined effects of earthquake and fire over time. Initially, for levels ranging from 20 % to 60 %, the curves start with relatively low probabilities of collapse, indicating a period of stability immediately after the earthquake, in contrast to the scenarios of load levels 70 % and 80 %, which exhibit significant probabilities of collapse at the inception of the fire, specifically 0.08 and 0.16, respectively. As time progresses, the probability of collapse increases for all scenarios, reflecting the progressive impact of fire on structural integrity. Critical timeframes can be identified where the probability of collapse accelerates rapidly. For example, beyond a certain threshold, there might be a sharp increase in collapse probability for buildings. These critical timeframes, observed at the instants of the median values of time to

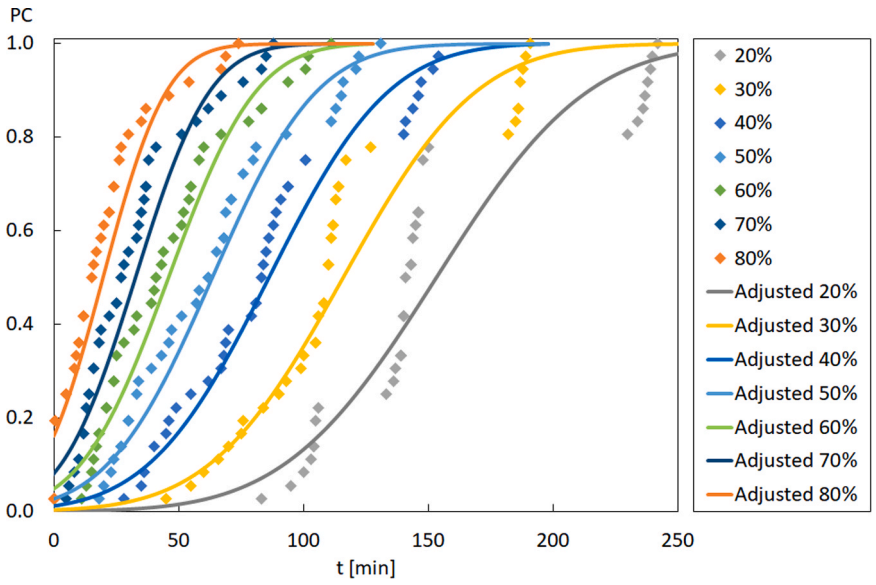

Fig. 28. - Probability of collapse as a function of time for the different load levels.

collapse, highlight periods of heightened risk where intervention or mitigation measures may be crucial to prevent collapse. Identifying and understanding these critical timeframes is crucial for risk assessment and the formulation of effective mitigation strategies. The comparison of the adjusted curves allows us to assess how the vertical loads influence the collapse probability. Buildings subjected to higher vertical loads demonstrate faster increases in collapse probability when compared to those with lower load levels.

Fig. 29 presents the evolution of collapse probability over time for various levels of story drift. Initially, for all story drift levels, curves may indicate minimal probabilities of collapse, suggesting structural stability shortly after the onset of seismic action. Notably, there is not a significant difference between the cases, especially between 2 % and 3 %, indicating a relatively consistent pattern across various levels of story drift.

Fig. 30 illustrates the probability of collapse as a function of time for the different fire scenarios. At the onset, each curve might display conservative probabilities of collapse, suggesting an initial period of structural stability. The fire scenario S3, characterised by the presence of fire on both the first and second levels, exhibits a notably elevated probability of collapse compared to other scenarios. The likelihood of collapse observed in fire scenario S1 is higher than that of scenario S2, as expected.

Fig. 31 depicts the progression of collapse probability over time, considering the damage type. Remarkably, the intact section scenario manifests the lowest probability of collapse, contrasting with the higher probabilities observed in the scenarios of damage A and damage B. Notably, a minor discrepancy emerges between damage scenarios A and B, with the latter exhibiting a slightly elevated likelihood of collapse.

It should be noted that across all figures, there is a potential for collapse upon ignition of the fire, indicating the necessity of considering the impact of FAE in the design of RC structures.

7. Conclusions

This study conducted comprehensive computational analyses to evaluate the behaviour of Reinforced Concrete (RC) structures under the influence of Fire After Earthquake (FAE) events. Key parameters

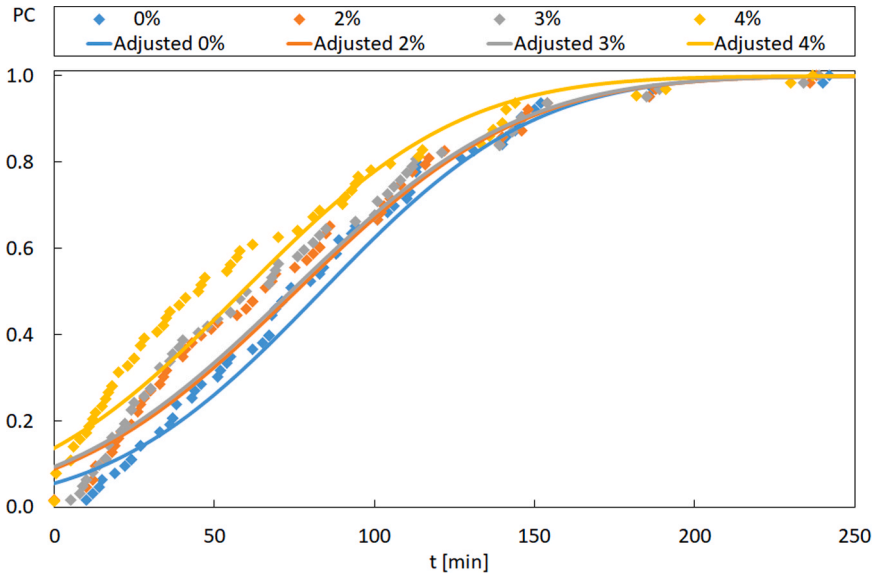

Fig. 29. - Probability of collapse as a function of time for the different story drifts.

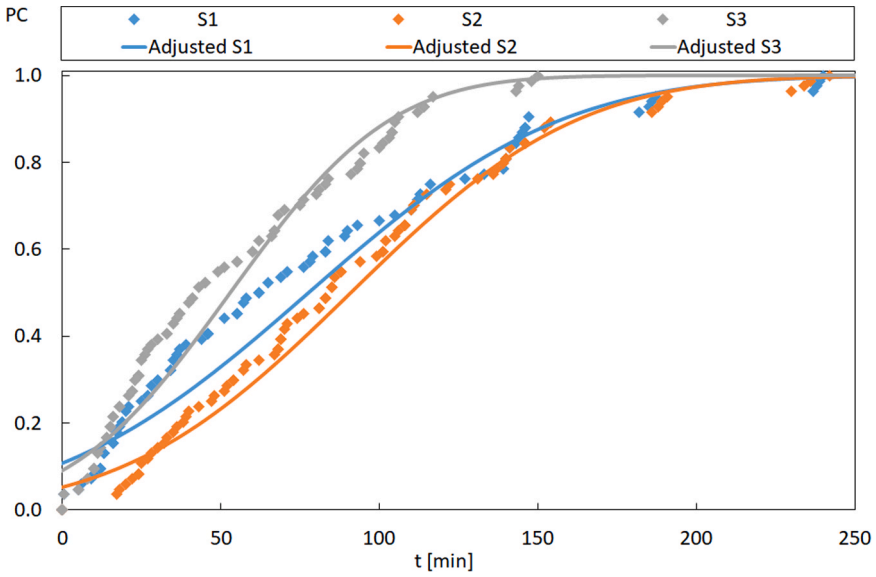

Fig. 30. - Probability of collapse as a function of time for the different fire scenarios.

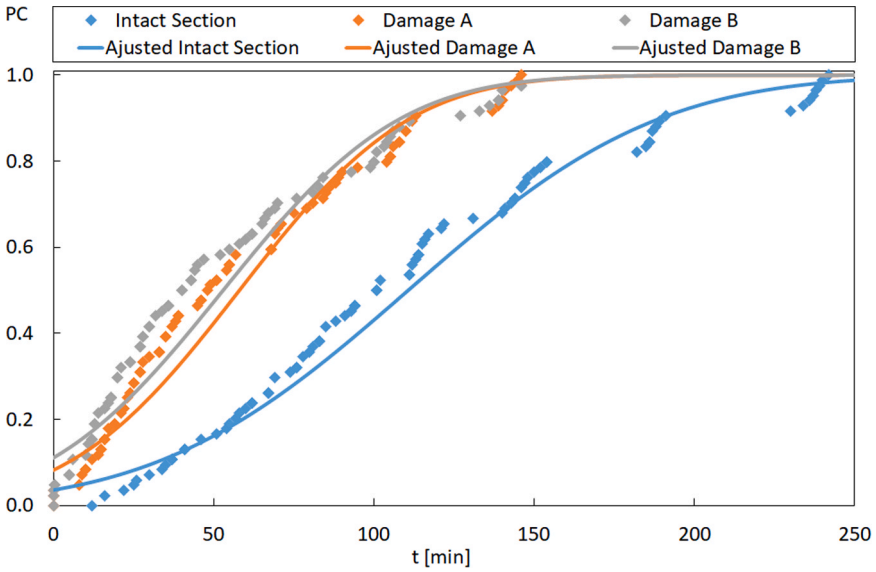

Fig. 31. - Probability of collapse as a function of time for the different types of damage.

considered in this investigation include vertical load, story drift, type of damage, and fire scenario. These parameters were systematically varied to assess their individual and collective effects on the structural behaviour of RC buildings subjected to FAE actions.

Fire scenario S1 demonstrates a greater likelihood of collapse than scenario S2, underscoring the critical influence of fire location and intensity on structural integrity. However, fire scenario S3, characterised by fire on both the first and second levels, presents a significantly elevated probability of collapse when compared to these alternative scenarios.

Across different levels of story drift, collapse probabilities exhibit minimal dispersion, especially between 2 % and 3 % drift levels, suggesting a consistent pattern irrespective of drift extent. This uniform pattern underscores the significance of the effect of such a parameter under FAE actions.

In the intact section, the lowest probability of collapse is observed, emphasising the crucial role of maintaining structural integrity in reducing collapse risk. Conversely, when any damage type A or B is present, the fire resistance decreases significantly, ranging from a minimum of 40 % to a maximum of 73 %, depending on the extent of story drift. The highest reduction values are associated with a 4 % story drift (SD). Additionally, damage scenarios A and B show slightly higher probabilities of collapse, with damage type A exhibiting a slightly lower probability when compared to damage type B.

Higher load levels typically decrease fire resistance, with a faster increase in the collapse probability due to FAE. While scenarios with load levels ranging from 20 % to 60 %, initially exhibit stability, significant probabilities of collapse emerge at the onset of fires in scenarios with 70 % and 80 %. Identifying critical timeframes, observed at median values of time to collapse, highlights periods of heightened risk requiring prompt intervention or mitigation strategies to avert collapse events.

CRediT authorship contribution statement

Ismail Haouach: Writing – original draft, Software, Methodology,

Investigation, Formal analysis, Conceptualization. **Abdelhak Kada:** Writing – review & editing, Software, Resources, Conceptualization. **Belkacem Lamri:** Writing – review & editing, Supervision, Conceptualization. **Paulo A. G. Piloto:** Writing – review & editing, Supervision, Conceptualization.

Declaration of Competing Interest

The authors declare that they have no known competing financial interests or personal relationships that could have appeared to influence the work reported in this paper.

Data availability

Data will be made available on request.

Appendix

Table A.1
Time to collapse of the studied structure considering all parameters.

Model	% of the load bearing capacity	Story drift	Cross section (Intact section/Damage A/ Damage B)	Fire scenario	Time until collapse (min)
1	80%	4%	Damage A	1	0
2	80%	2%	Damage B	1	0
3	80%	4%	Damage A	2	0
4	80%	4%	Damage B	2	0
5	80%	4%	Damage A	3	0
6	80%	2%	Damage B	3	0
7	80%	4%	Damage B	1	0.45
8	80%	4%	Damage B	3	0.45
9	80%	4%	Damage B	1	5
10	70%	4%	Damage B	3	5
11	80%	3%	Damage B	3	5
12	70%	4%	Damage B	1	6
13	70%	4%	Damage A	3	8
14	80%	3%	Damage A	3	8
15	80%	3%	Damage A	1	9
16	70%	4%	Damage A	1	10
17	70%	3%	Damage B	3	10
18	80%	2%	Damage A	3	10
19	80%	0%	Damage B	3	10
20	60%	4%	Damage B	3	11
21	70%	3%	Damage B	1	12
22	80%	2%	Damage A	1	12
23	80%	0%	Damage B	1	12
24	70%	2%	Damage B	3	12
25	80%	4%	Intact section	3	12
26	60%	4%	Damage B	1	13
27	70%	2%	Damage B	1	13
28	70%	3%	Damage A	3	14
29	70%	0%	Damage B	3	14
30	60%	4%	Damage A	3	15
31	80%	0%	Damage A	3	15
32	70%	3%	Damage A	1	16
33	80%	4%	Intact section	1	16
34	60%	3%	Damage B	3	16
35	70%	2%	Damage A	3	16
36	60%	4%	Damage A	1	17
37	80%	3%	Damage B	2	17
38	60%	3%	Damage B	1	18
39	70%	4%	Damage B	2	18
40	50%	4%	Damage B	3	18
41	60%	2%	Damage B	3	18
42	70%	2%	Damage A	1	19
43	80%	0%	Damage A	1	19
44	50%	4%	Damage B	1	20
45	80%	2%	Damage B	2	20
46	60%	2%	Damage B	1	21
47	60%	3%	Damage A	3	21
48	80%	3%	Damage A	2	22
49	70%	0%	Damage A	3	22
50	80%	3%	Intact section	3	22
51	50%	4%	Damage A	3	23
52	80%	2%	Damage A	2	24
53	80%	0%	Damage B	2	24
54	50%	3%	Damage B	3	24
55	60%	2%	Damage A	3	24
56	60%	0%	Damage B	3	24

(*continued on next page*)

Table A.1 (*continued*)

Model	% of the load bearing capacity	Story drift	Cross section (Intact section/Damage A/ Damage B)	Fire scenario	Time until collapse (min)
57	60%	3%	Damage A	1	25
58	70%	4%	Damage A	2	25
59	70%	4%	Intact section	3	25
60	80%	2%	Intact section	3	26
61	50%	4%	Damage A	1	27
62	70%	0%	Damage B	1	27
63	80%	0%	Damage A	2	27
64	50%	2%	Damage B	3	27
65	60%	2%	Damage A	1	28
66	70%	3%	Damage B	2	28
67	40%	4%	Damage B	3	28
68	50%	3%	Damage B	1	30
69	80%	3%	Intact section	1	30
70	70%	2%	Damage B	2	30
71	50%	3%	Damage A	3	30
72	60%	4%	Damage B	2	32
73	70%	3%	Damage A	2	33
74	50%	2%	Damage A	3	33
75	60%	0%	Damage A	3	33
76	50%	2%	Damage B	1	34
77	70%	4%	Intact section	1	34
78	80%	2%	Intact section	1	35
79	70%	2%	Damage A	2	35
80	40%	4%	Damage A	3	35
81	40%	4%	Damage B	1	36
82	70%	0%	Damage B	2	36
83	40%	3%	Damage B	3	36
84	70%	0%	Damage A	1	37
85	70%	3%	Intact section	3	37
86	80%	0%	Intact section	3	37
87	70%	0%	Damage A	2	38
88	50%	3%	Damage A	1	39
89	60%	4%	Damage A	2	39
90	60%	3%	Damage B	2	40
91	40%	2%	Damage B	3	40
92	60%	4%	Intact section	3	41
93	70%	2%	Intact section	3	41
94	60%	2%	Damage B	2	43
95	50%	0%	Damage B	3	43
96	60%	0%	Damage B	1	44
97	30%	4%	Damage B	3	45
98	40%	3%	Damage A	3	45
99	40%	4%	Damage A	1	46
100	50%	2%	Damage A	1	46
101	80%	0%	Intact section	1	46
102	50%	4%	Damage B	2	47
103	60%	3%	Damage A	2	48
104	40%	2%	Damage A	3	49
105	70%	3%	Intact section	1	51
106	60%	2%	Damage A	2	51
107	50%	0%	Damage A	3	51
108	60%	0%	Damage B	2	52
109	60%	0%	Damage A	2	54
110	80%	4%	Intact section	2	54
111	40%	3%	Damage B	1	55
112	60%	0%	Damage A	1	55
113	30%	4%	Damage A	3	55
114	60%	3%	Intact section	3	55
115	70%	2%	Intact section	1	57
116	50%	4%	Damage A	2	57
117	60%	4%	Intact section	1	58
118	50%	3%	Damage B	2	58
119	30%	3%	Damage B	3	60
120	60%	2%	Intact section	3	60
121	40%	2%	Damage B	1	62
122	70%	0%	Intact section	1	62
123	50%	2%	Damage B	2	62
124	50%	4%	Intact section	3	62
125	50%	0%	Damage B	1	65
126	30%	2%	Damage B	3	66
127	80%	3%	Intact section	2	67
128	40%	0%	Damage B	3	67
129	60%	0%	Intact section	3	67
130	70%	0%	Intact section	3	67
131	50%	2%	Damage A	2	68
132	50%	3%	Damage A	2	68

(*continued on next page*)

Table A.1 (*continued*)

Model	% of the load bearing capacity	Story drift	Cross section (Intact section/Damage A/ Damage B)	Fire scenario	Time until collapse (min)
133	40%	0%	Damage A	3	68
134	40%	3%	Damage A	1	69
135	50%	0%	Damage B	2	69
136	80%	2%	Intact section	2	69
137	40%	4%	Damage B	2	70
138	30%	3%	Damage A	3	70
139	50%	0%	Damage A	1	71
140	50%	0%	Damage A	2	71
141	80%	0%	Intact section	2	74
142	30%	2%	Damage A	3	75
143	30%	4%	Damage B	1	76
144	70%	4%	Intact section	2	76
145	50%	3%	Intact section	3	76
146	60%	3%	Intact section	1	78
147	40%	2%	Damage A	1	79
148	50%	0%	Intact section	3	80
149	40%	4%	Damage A	2	81
150	40%	3%	Damage B	2	81
151	50%	2%	Intact section	3	81
152	60%	0%	Intact section	1	83
153	60%	2%	Intact section	1	83
154	40%	2%	Damage B	2	83
155	70%	3%	Intact section	2	83
156	20%	4%	Damage B	3	83
157	40%	0%	Damage B	1	84
158	30%	0%	Damage A	3	84
159	40%	3%	Damage A	2	85
160	70%	2%	Intact section	2	85
161	40%	2%	Damage A	2	86
162	40%	0%	Damage A	2	88
163	70%	0%	Intact section	2	88
164	40%	0%	Damage A	1	89
165	30%	4%	Damage A	1	90
166	40%	4%	Intact section	3	91
167	50%	4%	Intact section	1	93
168	30%	0%	Damage B	3	93
169	60%	4%	Intact section	2	94
170	40%	0%	Intact section	3	94
171	40%	3%	Intact section	3	94
172	20%	4%	Damage A	3	95
173	30%	4%	Damage B	2	99
174	30%	3%	Damage B	1	100
175	20%	3%	Damage B	3	100
176	40%	0%	Damage B	2	101
177	60%	3%	Intact section	2	101
178	40%	2%	Intact section	3	101
179	60%	2%	Intact section	2	102
180	20%	2%	Damage B	3	103
181	20%	3%	Damage A	3	104
182	20%	0%	Damage B	3	104
183	30%	2%	Damage B	1	105
184	30%	4%	Damage A	2	105
185	20%	2%	Damage A	3	105
186	30%	3%	Damage B	2	106
187	20%	0%	Damage A	3	106
188	30%	2%	Damage A	2	108
189	30%	3%	Damage A	2	108
190	30%	2%	Damage B	2	108
191	30%	3%	Damage A	1	110
192	30%	0%	Damage A	2	110
193	50%	0%	Intact section	1	111
194	30%	0%	Damage B	2	111
195	60%	0%	Intact section	2	111
196	30%	2%	Damage A	1	112
197	30%	3%	Intact section	3	112
198	30%	0%	Damage A	1	113
199	50%	3%	Intact section	1	113
200	30%	0%	Intact section	3	114
201	30%	4%	Intact section	3	114
202	50%	4%	Intact section	2	115
203	50%	2%	Intact section	1	116
204	30%	2%	Intact section	3	117
205	50%	3%	Intact section	2	121
206	50%	2%	Intact section	2	122
207	30%	0%	Damage B	1	127
208	50%	0%	Intact section	2	131

(*continued on next page*)

Table A.1 (*continued*)

Model	% of the load bearing capacity	Story drift	Cross section (Intact section/Damage A/ Damage B)	Fire scenario	Time until collapse (min)
209	20%	4%	Damage B	1	133
210	20%	4%	Damage B	2	136
211	20%	4%	Damage A	2	137
212	20%	2%	Damage B	1	139
213	20%	3%	Damage B	1	139
214	20%	3%	Damage A	2	139
215	20%	4%	Damage A	1	140
216	20%	0%	Damage B	1	140
217	20%	2%	Damage A	2	140
218	40%	4%	Intact section	2	140
219	40%	4%	Intact section	1	141
220	20%	0%	Damage A	2	141
221	20%	3%	Damage A	1	143
222	20%	3%	Intact section	3	143
223	40%	0%	Intact section	1	144
224	20%	4%	Intact section	3	144
225	20%	0%	Damage A	1	145
226	20%	2%	Damage A	1	146
227	40%	3%	Intact section	1	146
228	20%	0%	Damage B	2	146
229	20%	2%	Damage B	2	146
230	20%	3%	Damage B	2	146
231	40%	2%	Intact section	1	147
232	20%	2%	Intact section	3	148
233	20%	0%	Intact section	3	150
234	40%	0%	Intact section	2	152
235	40%	2%	Intact section	2	154
236	40%	3%	Intact section	2	154
237	30%	4%	Intact section	1	182
238	30%	3%	Intact section	1	185
239	30%	2%	Intact section	1	186
240	30%	0%	Intact section	2	186
241	30%	0%	Intact section	1	187
242	30%	2%	Intact section	2	188
243	30%	3%	Intact section	2	189
244	30%	4%	Intact section	2	191
245	20%	4%	Intact section	2	230
246	20%	3%	Intact section	2	234
247	20%	2%	Intact section	2	236
248	20%	4%	Intact section	1	237
249	20%	2%	Intact section	1	238
250	20%	3%	Intact section	1	239
251	20%	0	Intact section	1	240
252	20%	0%	Intact section	2	242

References

[1] Behnam B. Post-earthquake fire analysis in urban structures: risk management strategies. CRC Press; 2017.

[2] Behnam B, Ronagh H. Performance-based vulnerability assessment of multi-story reinforced concrete structures exposed to pre-and post-earthquake fire. J Earthq Eng 2014;18(6):853–75.

[3] Behnam B, Ronagh H. An engineering solution to improve post-earthquake fire resistance in important reinforced concrete structures. Adv Struct Eng 2014;17(7):993–1009.

[4] Merouani MR, et al. Mechanical analysis of a portal steel frame when subjected to a post-earthquake fire. Fire Res 2019;3(1).

[5] Merouani MR, et al. Finite-element analysis for the performance of steel frames under fire after earthquake. Asian J Civ Eng 2022.

[6] Mostafaei H, Kabeyasawa T. Performance of a six-story reinforced concrete structure in post-earthquake fire. 10th Canadian Conference on Earthquake Engineering. Toronto, Ontario: Institute for Research in Construction,; 2010.

[7] Kumar, V., et al. *Behaviour of full-scale reinforced concrete frame under simulated post-earthquake fire*. in *Proc., 15th World Conf. on Earthquake Engineering*. 2012.

[8] Ab-Kadir, M.A., et al. *Modelling of an earthquake damaged RC frame subjected to fire*. in *Proceedings of 7th international conference on structures in fire*. 2012.

[9] Behnam B, Ronagh HR, Baji H. Methodology for investigating the behavior of reinforced concrete structures subjected to post earthquake fire. Adv Concr Constr 2013;1(1):29.

[10] Ni S, Birely AC. Impact of physical seismic damage on the fire resistance of reinforced concrete walls. Constr Build Mater 2018;182:469–82.

[11] Vitorino H, Rodrigues H, Couto C. Evaluation of post-earthquake fire capacity of reinforced concrete elements. Soil Dyn Earthq Eng 2020;128:105900.

[12] Manish H, Swathi M, Kumari SA. Behaviour of RC Frame Subjected to Fire Following Earthquake. Seismic Design and Performance: Select Proceedings of 7th ICRAGEE 2020. Springer,; 2021. p. 335–46.

[13] Vitorino H, et al. Post-Earthquake Fire Assessment of Reinforced Concrete Frame Structures. Structural Engineering International,; 2022. p. 1–15.

[14] CEN. EN 1998-1: design of structures for earthquake resistance. *Brussels, Belgium*: European Committee for Standardization,; 2004.

[15] Lakhani H, et al. Thermal analysis of reinforced concrete structural elements. J Struct Fire Eng 2013.

[16] Zitouni M, Lamri B, Kada A. Fire resistance performance of glass fiber reinforced concrete columns. CIGOS 2021, Emerging Technologies and Applications for Green Infrastructure. Springer,; 2022. p. 275–83.

[17] CBA. Règles de Conception et de Calcul des Structures en Béton Armé. Centre National De Recherche Appliquée En Génie Parasismique,; 1993.

[18] Forcellini D. Seismic fragility of tall buildings considering soil structure interaction (SSI) effects. Structures 2022;45:999–1011.

[19] Fiamingo A, Bosco M, Massimino MR. The role of soil in structure response of a building damaged by the 26 December 2018 earthquake in Italy. J Rock Mech Geotech Eng 2023;15(4):937–53.

[20] CEN. EN 1363-1, Fire resistance tests, General requirements. *Brussels, Belgium*: European Committee for Standardization; 2020.

[21] RPA99v2003. Règles Parasismiques Algériennes 99 version 2003. Algeria: Centre National De Recherche Appliquée En Génie Parasismique,; 2003.

[22] Schneider U. Concrete at high temperatures—a general review. Fire Saf J 1988;13(1):55–68.

[23] Buchanan AH, Abu AK. Structural design for fire safety. John Wiley & Sons; 2017.

[24] CEN. EN 1992-1-2, Design of Concrete Structures, General Rules, Structural Fire Design. *Brussels, Belgium*: European Committee for Standardization,; 2004.

[25] CEN. EN 1994-1-2, Design of composite steel and concrete structures, General rules, Structural fire design. *Brussels, Belgium*: European Committee for Standardization; 2005.

[26] Krishna DA, Priyadarsini R, Narayanan S. Effect of elevated temperatures on the mechanical properties of concrete. Procedia Struct Integr 2019;14:384–94.
[27] Haouach I, Lamri B, Kada A. Investigación de la capacidad de fuego antes y post terremoto de una estructura de hormigón armado. Innovación Tecnológica y desarrollo sostenible en la edificación. Dykinson,; 2022.
[28] Haouach I, Lamri B, Kada A. Post-earthquake fire capacity assesment of a reinforced concrete frame. Anales de Edificación 2022;Vol. 8(Núm. 3):2022. https://doi.org/10.20868/ade.2022.5097.
[29] Kada A, Lamri B. Numerical analysis of non-restrained long-span steel beams at high temperatures due to fire. Asian J Civ Eng 2019;20(2):261–7.
[30] Kada A, et al. Finite element analysis of steel beams with web apertures under fire condiction. Asian J Civ Eng 2016;17(8):1035–54.
[31] Lamri B, et al. Behavior of cellular beams protected with intumescent coatings. Fire Res 2017;1(1).
[32] Oribi SB, et al. Investigation of residual stresses on the fire resistance of unrestrained cellular beams. ce/Pap 2021;4(2-4):1386–94.
[33] Kumar W, Sharma UK, Shome M. Mechanical properties of conventional structural steel and fire-resistant steel at elevated temperatures. J Constr Steel Res 2021;181:106615.
[34] CEN. EN 1991-1-2, Actions on Structures, General Actions, Actions on Structures Exposed to Fire. *Brussels, Belgium*: European Committee for Standardization,; 2002.
[35] Wolanski AJ. Flexural behavior of reinforced and prestressed concrete beams using finite element analysis. Citeseer,; 2004.
[36] Gao W, et al. Finite element modeling of reinforced concrete beams exposed to fire. Eng Struct 2013;52:488–501.
[37] Pires F. Influência das paredes de alvenaria no comportamento de estruturas reticuladas de betão armado sujeitas a acções horizontais. Lisboa: LNEC,; 1990.
[38] Braz-César, M., D.V. Oliveira, and R. Barros. *Comparison of cyclic response of reinforced concrete infilled frames with experimental results*. in *14 WCEE–14th World Conference on Earthquake Engineering* . 2008.
[39] Pires, F., *Influência das paredes de alvenaria no comportamento de estruturas reticuladas de betão armado sujeitas a acções horizontais*, in *LNEC*. 1990: Lisbon, Portugal.
[40] Dwaikat M, Kodur V. Response of restrained concrete beams under design fire exposure. J Struct Eng 2009;135(11):1408–17.
[41] ASTM, *Standard methods of fire test of building construction and materials*, in *E 119–08a*. 2008: West Conshohocken, Pa.
[42] Vitorino H, et al. Assessment of post-earthquake fire capacity of RC frames without seismic design. Eng Fail Anal 2024;160:108248.
[43] Dahal P, Mullen C. Incorporation of post-earthquake fire (PEF) and subsequent aftershock for performance analysis of steel buildings. Structures 2021;33:3810–21.